AN INVESTIGATION INTO THE LUMINESCENCE AND STRUCTURAL PROPERTIES OF ALKALI EARTH METANIOBATES

A Thesis
Presented to
The Academic Faculty

by

Ogundiran Soumonni

In Partial Fulfillment
of the Requirements for the Degree
Master of Science in Materials Science and Engineering

Georgia Institute of Technology
April 2004

AN INVESTIGATION INTO THE LUMINESCENCE AND STRUCTURAL PROPERTIES OF ALKALI EARTH METANIOBATES

Approved:

Dr. Christopher J. Summers, Advisor

Dr. Rosario A. Gerhardt

Dr. Meilin Liu

Dr. Brent K. Wagner

Date Approved: April 30, 2004

To my parents,

Elisée and Maria Soumonni

TABLE OF CONTENTS

Acknowledgements……vii

List of Tables……viii

List of Figures……ix

Summary…...……..……..…...……..xii

Chapter I Introduction……...……..……1

Chapter II Background……..…….....7

2.1 Luminescence……....7

2.2 Absorption……....10

2.3 Emission…….....13

2.4 Photoluminescence…….....16

2.5 Crystal Structure…….....18

2.6 Luminescence of Niobates and Tantalates…….....20

2.7 Solid State Synthesis……..…….....26

Chapter III Experimental Procedure…….…..….....28

3.1 Synthesis Procedure……..…….....28

3.2 Optimization of Synthesis Parameters……..…….....29

3.3 X-ray Diffraction……..…….....30

3.4 Photoluminescence Instrumentation……..…….....32

3.5 Photoluminescence and Photoluminescence Excitation.....35

3.6 Scanning Electron Microscopy……..…….....36

Chapter IV Results……..37

4.1 Optimization of Firing Temperature and Stoichiometry.....37

4.2 Structure and Chemical Analysis…….....40

4.2.1 X-Ray Diffraction of $Ca_{1-x}Sr_xNb_2O_6$….....42

4.2.2 X-Ray Diffraction of $Ca_{1-x}Zn_xNb_2O_6$….....44

4.2.3 X-Ray Diffraction of $CaNb_{2(1-x)}Ta_{2x}O_6$….....45

4.2.4 X-Ray Diffraction of $Ca_{1-x}Ba_xNb_2O_6$….....46

4.2.5 X-Ray Diffraction of $Ca_{1-x}Mg_xNb_2O_6$….....47

4.3 Optical Characterization…….....48

4.3.1 PL and PLE of $Ca_{1-x}Sr_xNb_2O_6$….....48

4.3.2 PL and PLE of $Ca_{1-x}Zn_xNb_2O_6$….....51

4.3.3 PL and PLE of $CaNb_{2(1-x)}Ta_{2x}O_6$….....54

4.3.4 PL and PLE of $Ca_{1-x}Ba_xNb_2O_6$….....56

4.3.5 PL and PLE of $Ca_{1-x}Mg_xNb_2O_6$….....58

4.4 Morphology and Particle Size…….....60

Chapter V Calculations…….....62

5.1 Stokes Shift Calculation…….....62

5.2 CIE coordinates…….....64

Chapter VI Discussion…….....67

6.1 Effect of Alloying on Structure.....67

6.2 Effect of Alloying on Luminescence.....69

Chapter VII Conclusion…….....72

Chapter IIX Reference…….....75

ACKNOWLEDGEMENTS

I wish to thank my advisor, Dr. C.J. Summers, for his guidance throughout the work on this thesis, and for providing the supervision, guidance and support throughout the course of my research. I would also like to thank Dr. R.A. Gerhardt, Dr. M. Liu and Dr. B.K. Wagner for serving as members of my committee and for contributing very useful thoughts and suggestions to my work. I am indebted to Dr. Chulsoo Yoon, Dr. Hisham Menkara and Richard Gilstrap for all their assistance in this research as well as useful discussions, and Xudong Wang for providing the low voltage SEM measurements.

Finally, I thank my parents, my sister, Lola and my friends for their continued support and encouragement.

LIST OF TABLES

Table 1.1 Current Plasma Phosphors……2

Table 3.1 Optimization of Stoichiometry and Firing temperature…….....29

Table 4.1 Synthesis of Solid Solutions……..40

Table 5.1. The CIE coordinates of the spectrally pure colors, which are placed at the end points of the diagram…….....65

LIST OF FIGURES

Figure 1.1 (a) represents the unit cell of Calcium Metaniobate; black circles; black circles are calcium; open circles are niobium……...…….5

Figure 1.1 (b) Simplified representation showing a distorted perovskite cube (cuboid) of Ca atoms surrounding one niobate octahedron……5

Figure 2.1.a Physical model of luminescence, where Exc: Excitation, EM: Emission or radative return to the ground state, HEAT: Non-radiative return to the ground state…….8

Figure 2.1.b. Energy Level Diagram of processes in A, where A*: Excited State of Activator, A: Ground State of Activator, R: Radiative return to the ground state or emission, NR: Non-radiative return to the ground state or heat……..8

Figure 2.2. Structure of $Ca_2Nb_2O_7$ showing projection down [010] showing two successive slabs of $Ca_2Nb_2O_7$ parallel to (100). Slabs are drawn in their idealized perovskite form. The Ca ions and NbO_6 octahedra in light and heavy outline lie at y = _ and y = _ respectively. Distortions from this idealized structure are listed in the text. The broken lines and arrows show the projection of the true monoclinic unit cell……..18

Figure 2.3. An artist's conception of the octahedral arrangement of oxygen atoms surrounding calcium and niobium atoms in the unit cell of calcium niobate; black circles are calcium; open circles are niobium. There are four calcium, eight niobium and twenty four oxygen atoms per unit cell…….20

Figure 3.1 Arrangement of photoluminescence spectroscopy system……...34

Figure 4.1 Photoluminescence of Various Compositions of $CaNb_2O_6$ Fired at 1300 °C and 1200 °C…….....38

Figure 4.2 Photoluminescence of various compositions of $CaNb_2O_6$ fired at 1200 °C……..39

Figure 4.3 PLE of various compositions of $CaNb_2O_6$ at 1200 °C…….39

Figure 4.4 Calcium Metaniobate fired at 1200 °C. Blue luminescence……41

Figure 4.5. X-ray diffraction spectra of $Ca_{1-x}Sr_xNb_2O_6$ for x = 0.1 to x = 0.5……...43

Figure 4.6. X-ray diffraction spectra of $Ca_{1-x}Zn_xNb_2O_6$ for x = 0 to x = 0.4…….44

Figure 4.7. X-ray diffraction spectra of $CaNb_{2(1-x)}Ta_{2x}O_6$ for x = 0.1 to x = 1……..45

Figure 4.8. X-ray diffraction spectra of $Ca_{1-x}Ba_xNb_2O_6$ for x = 0.1 to x = 0.3……..46

Figure 4.9. X-ray diffraction spectra of $Ca_{1-x}Mg_xNb_2O_6$ for x = 0.1 to x = 0.3…….47

Figure 4.10. Photoluminescence spectra of $Ca_{1-x}Sr_xNb_2O_6$……...50

Figure 4.11. Photoluminescence excitation spectra of $Ca_{1-x}Sr_xNb_2O_6$……..50

Figure 4.12. Photoluminescence spectra of $Ca_{1-x}Zn_xNb_2O_6$……..53

Figure 4.13. Photoluminescence Excitation spectra of $Ca_{1-x}Zn_xNb_2O_6$…….53

Figure 4.14. PL spectra of $CaNb_{2x}Ta_{2(1-x)}O_6$.....55

Figure 4.15. Photoluminescence excitation spectra of $CaNb_{2x}Ta_{2(1-x)}O_6$……..55

Figure 4.16. Photoluminescence spectra of $Ca_{1-x}Ba_xNb_2O_6$……..57

Figure 4.17. Photoluminescence excitation spectra of $Ca_{1-x}Ba_xNb_2O_6$…….57

Figure 4.18. Photoluminescence spectra of $Ca_{1-x}Mg_xNb_2O_6$…….59

Figure 4.19. Photoluminescence excitation spectra of $Ca_{1-x}Mg_xNb_2O_6$……....59

Figure 3.1a shows an SEM picture of $Ca_{0.8}Sr_{0.2}Nb_2O_6$ at 1570, X magnification showing loosely agglomerated particles…….……60

Figure 3.1b shows an SEM picture of $Ca_{0.8}Sr_{0.2}Nb_2O_6$ at 13,500 X magnification showing more distinct particles…….……....61

Figure 5.1 Excitation and emission spectra of the intrinsic luminescence of $CaNb_2O_6$ showing Stokes' shift……...63

Figure 5.2 CIE chromaticity diagram showing coordinates of $Ca_{0.8}Sr_{0.2}Nb_2O_6$ (x = 0.2295, y = 0.30467) lying on the edge of blue-green and leaning strongly towards white, while BAM (x = 0.15, y = 0.086) strongly lies in the blue regime……66

SUMMARY

A comprehensive investigation was reported into the synthesis, characterization and photoluminescence properties of calcium metaniobates and associated alkali earth alloy systems. Previous studies have shown that calcium metaniobate exhibits a strong self-activated blue luminescence at room temperature in stark contrast to the pyroniobates which are known to exhibit a temperature dependent luminescence that quenches above 100 K. The mechanism of this behavior has been studied by measuring the spectral characteristics of the photoluminescence and photoluminescence excitation spectra on the crystalline and morphological properties of the powders as determined from x-ray diffraction and scanning electron microscopy. By correlating the synthesis parameters with the physical, chemical and optical properties of calcium metaniobate, the optimum conditions for efficient blue-visible emission and chemical stability under vacuum ultraviolate (VUV) radiation has been determined. These materials have the potential to replace Barium Magnesium Aluminate, which is currently used as the blue phosphor in plasma displays.

CHAPTER I

INTRODUCTION

Plasma display panels (PDPs) are currently the only viable display technology for large screens with a larger than 60” diagonal. This kind of display makes use of a xenon plasma discharge, which generates high-energy photons that in turn excite the phosphors to obtain the primary colors of red, blue and green. The excitation wavelengths employed are 147 nm and 172nm. This high energy requirement in PDPs makes it necessary to develop novel phosphors that display strong absorption at the plasma excitation wavelengths, can produce an efficient energy transfer from the host lattice to the activator ions, and which have the proper crystal field environment which allows the emission of visible photons with the desired chromaticity. Due to the harsh operational environment of high energy VUV radiation and ion bombardment, it is necessary that PDP materials be able to withstand this energy and remain stable during panel manufacture.

The current plasma phosphors being used are shown in Table 1 below.

Table 1.1 Current Plasma Phosphors

	Red	Green	Blue
Phosphor	$(Y,Gd)BO_3:Eu^{3+}$	$ZnSiO_4$: Mn^{2+}	$BaMgAl_{14}O_{23}$: Eu^{2+}(BAM)
Peak Position	620 nm	520 nm	452 nm
CIE chromaticity coordinates	x = 0.641 y = 0.356	x = 0.242 y = 0.708	x = 0.147 y = 0.067
Decay time	9 ms	14 ms	<1 ms
Performance due to high energy ion bombardment	Stable	Stable	Unstable

These phosphors all possess the desired emission wavelengths and required CIE chromaticity coordinates. The red and blue phosphors also possess adequate decay time and the green is marginally adequate. However, while the red and green phosphors are stable during panel manufacture, the blue $BaMgAl_{10}O_{17}$: Eu^{2+} is unstable and has a poor thermal performance following the burn-in procedure used in manufacturing the panels.

Thus, one of the major challenges in display technology today is to design a novel blue plasma display phosphor that displays good thermal stability while at the same time emitting efficiently at the desired wavelength and color coordinates. Recent experimental work has shown that the $CaSrP_2O_7$: Eu^{2+} phosphor has a much better thermal performance following burn-in than the currently used BAM.[19] However, because the host sensitization band of this compound is not properly positioned with respect to the primary excitation line of 147 nm used in plasma displays, it was necessary to improve this phosphor or alternatively, develop another one that combines the stability requirement and the emission requirement. In order to preserve the crystal structure of $CaSrP_2O_7$:Eu^{2+} that satisfies the stability requirement, it was proposed that niobium (Nb) or tantalum (Ta) be substituted so as to replace phosphorus (P) since Nb and Ta belong to group 5B and have the same valency as P, which belongs to group 5A. This is the motivation for the present thesis and a comprehensive investigation into niobates and tantalates has been carried out to observe how the host lattices of these compounds absorb VUV energy, what emission processes take place and to verify whether they satisfy the blue phosphor requirement in plasma displays. The development of phosphors that are designed to be used in a new lamp generation such as Xe lamps, which are

excited in the VUV range has also been reported.[23,24] This provided an additional incentive to purse this research.

A preliminary investigation of the pyroniobates, $M_2Nb_2O_7$ where M=Ca, Sr, Ba, showed that the luminescence in these compounds is completely quenched at room temperature. A mixed phase of $Ca_2Nb_2O_7$ and $CaNb_2O_6$ was found to be luminescent but upon synthesizing the single phase of $CaNb_2O_6$, it was found to be responsible for the room temperature luminescence. Some other metaniobates such as those of Cd, Zn and Mg are also known to be luminescent at room temperature. $CaNb_2O_6$ is a self-activated blue phosphor in which Eu^{3+} can be incorporated into the host lattice thereby producing a red phosphor. However, we were unable to reduce the Eu^{3+} to Eu^{2+} to obtain a blue phosphor and so it became necessary to try to affect the "self –activated" or intrinsic property of this phosphor. This is the framework under which the present work was carried out.

The emission band of the self-activated $CaNb_2O_6$ was found to be at 464.5 nm and the excitation band showed absorption at excitation wavelengths as low as 147 nm, but with the strongest absorption occurring within the range of 200 nm to 260 nm. Based on these characteristics, three major directions have been proposed in this thesis to control the chromaticity of this phosphor.

1.) Alloying $CaNb_2O_6$ with an alkali earth cation that would substitute for a Ca^{2+} site in the lattice: The luminescent centers in this material are NbO_6^{2-} octahedra surrounded by an irregular cuboid of Ca atoms. Therefore, using a larger atom would expand the lattice (cuboid), which would increase the crystal field that the luminescent center experiences and which could also shift the emission band to

slightly lower wavelengths. According to their atomic radii, alloying elements such as Mg (0.65 A°), Sr (1.13 A°), and Ba (1.35 A°), could be used, but Sr was selected because it is only slightly larger than Ca (0.99 A°) and has the highest probability of filling in a Ca^{2+} position in the structure. A picture of the unit cell of $CaNb_2O_6$ and an oversimplified, but representative figure of the basic idea are shown in Figure 1.1a and Figure 1.1 b respectively.

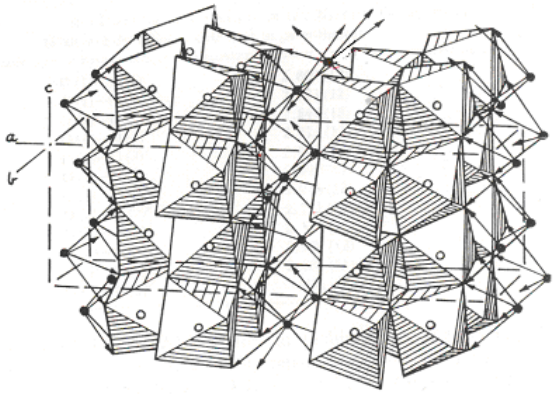

Figure 1.1 (a)

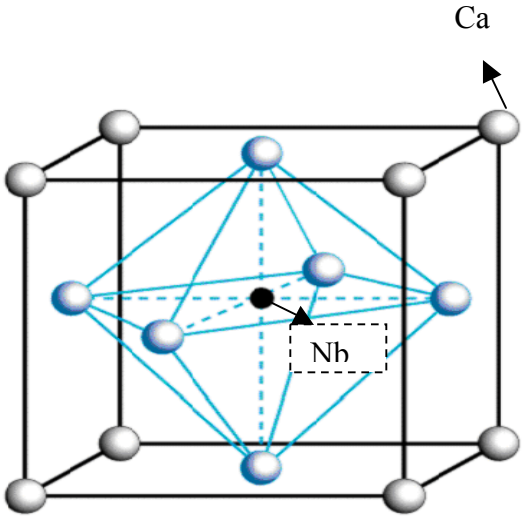

Figure 1.1 (b)

Figure 1.1 (a) represents the unit cell of Calcium Metaniobate; black circles; black circles are calcium; open circles are niobium
Figure 1.1 (b) Simplified representation showing a distorted perovskite cube (cuboid) of Ca atoms surrounding one niobate octahedron.

2.) Alloying $CaNb_2O_6$ with another M^{2+} cation with a large amount of d electrons: It has been proposed in the literature that d electrons in an M^{2+} ion of MNb_2O_6, such as Cd (0.97) A°, favor the delocalization of the electrons belonging to the niobate group relative to that of Ca^{2+}. [5] Zn (0.74 A°) is actually smaller in size than Ca (0.99 A°) and based on the purely electrostatic interactions considered in the first

approach, it would appear initially that its substitution would cause a contraction in the lattice leading to a decrease in the crystal field experienced by the luminescent center and hence a reduction in the intensity of the emission. However, Zn^{2+} (a transition metal ion) has a different chemical nature than the alkali earth metals and its delocalized d electrons might be able to participate in the O^{2-} to Nb^{5+} charge transfer, which would enhance the luminescence intensity.

3.) Alloying $CaNb_2O_6$ with Ta: The third approach which appears to be the most promising method of affecting the self-activated luminescence of $CaNb_2O_6$ combines the first two approaches, but more importantly modifies the NbO_6 group, which is the luminescent center in this phosphor. By alloying Nb (0.78 A°) with Ta (0.78 A°), which has the same crystal structure and the same ionic size within the octahedral configuration (but Ta has a slightly larger atomic size), we expect a lattice expansion with a corresponding increase in the crystal field the luminescent center experiences and hence an increase in intensity. Secondly, Ta has d electrons that could participate in the O^{2-} to Nb^{5+} charge transfer and which could also enhance the luminescence intensity. Finally, it has been reported that the excitation and emission maxima of the tantalates are always at higher energies than those of the corresponding niobates due to the higher 5^{th} ionization potential of tantalum in comparison with niobium.[2] Thus, as a consequence of the alloying, we expect a shift in the maximum excitation band to lower wavelengths, a shift in the emission band to a lower and more suitable emission wavelength, as well as an increase in the intensity of the emission.

CHAPER II

BACKGROUND

2.1 Luminescence

A luminescent material or phosphor is a solid that converts certain types of energy into electromagnetic radiation over and above thermal radiation.[8] Even though the electromagnetic radiation emitted by a phosphor is usually in the visible range, it can also be in other spectral regions such as the UV or infrared.

Luminescence can be classified according to the different types of energy used to excite the phosphor namely:

1.) Photoluminescence, which involves excitation by an electromagnetic radiation that is usually UV radiation.
2.) Cathodoluminescence, which is excitation by a beam of energetic electrons
3.) Electroluminescene occurs when the source of excitation is an electric voltage
4.) Triboluminescence, which is produced by mechanical energy such as grinding
5.) X-ray Luminescence, when excitation is by x-rays
6.) Chemiluminescence, when the material is excited by the energy of a chemical reaction.

In the general mechanism of luminescence, the activator absorbs the exciting radiation, which then raises it to an excited state. This excited state then returns to the ground state by the emission of radiation: a photon. Competing with this process are processes that occur when the energy of the excited state excites the lattice vibrations, or phonons, to heat the host lattice. These two forms of radiation are competitive and

so in order to design an efficient phosphor, the non-radiative process has to be suppressed. A schematic of such a process is shown below.

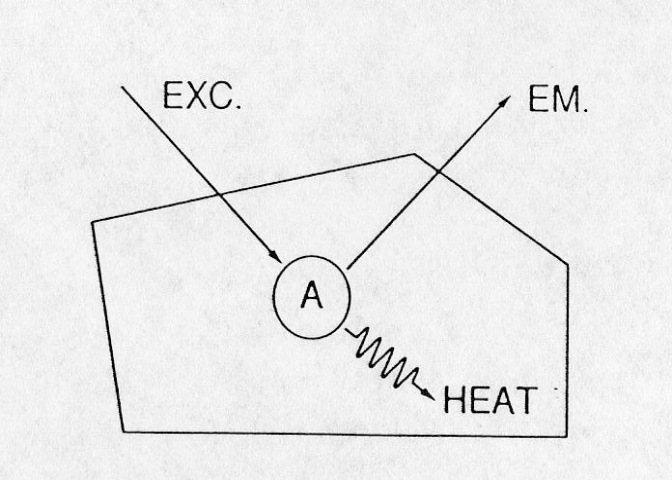

Figure 2.1.a Physical model of luminescence, where Exc: Excitation, EM: Emission or radative return to the ground state, HEAT: Non-radiative return to the ground state.

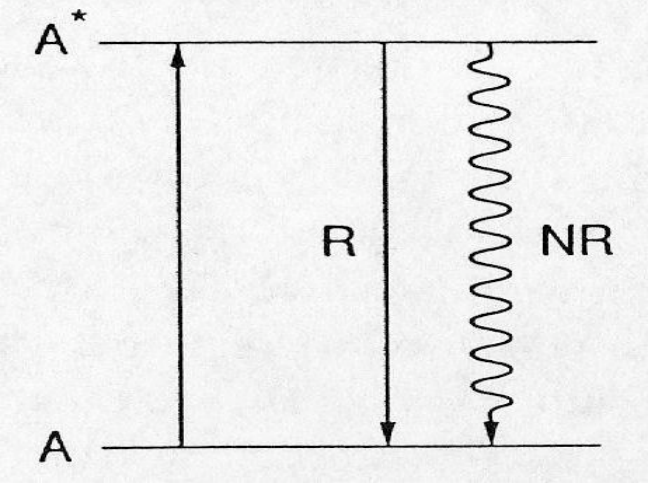

Figure 2.1.b. Energy Level Diagram of processes in (a), where A*: Excited State of Activator, A: Ground State of Activator, R: Radiative return to the ground state or emission, NR: Non-radiative return to the ground state or heat.

In the simple mechanism described above and shown in figures 2.1a and 2.1 b, the host lattice does not participate in optical processes, but simply "holds" the activator ion tightly while the activator absorbs the energy and emits the radiation. A well-known example is ruby, $Al_2O_3:Cr^{2+}$, and $Y_2O_3:Eu^{3+}$. However, if another ion is added to the host lattice, this ion may absorb the excitation energy and then transfer it to the activator. Such an absorbing ion is known as a sensitizer. In $Ca_5(PO_4)_3F:Sb^{3+},Mn^{2+}$, for example, the UV radiation is only absorbed by the Sb^{3+} due to an energy transfer composed partly of the blue Sb^{3+} emission and partly of the Mn^{2+} emission.[8]

Generally, the concentration of the activator or luminescent center is of the order of 1 mol % and the centers are approximated as being randomly distributed throughout the host lattice. However, the activator concentration can sometimes be 100 % in which case, the activator ion or group is both a luminescent center and a building unit of the host lattice. A well-known example is $CaWO_4$ where the tungstate group (WO_4^{2-}) is the luminescent center and $CaNb_2O_6$ where the niobate octahedron ($Nb_2O_6^{2-}$) is the luminescent center. This class of phosphors is known as "self-activated" because the host lattice both absorbs and emits the radiation.

Another mechanism of luminescence is one in which the host lattice is excited and then transfers its excitation energy to the activator. In this case, the host lattice acts as a sensitizer and this mechanism is typical of high-energy excitation, such as by x-rays or cathodoluminescence. One example is $YVO_4:Eu^{3+}$ in which the vanadate group (VO_4^{3-}) in the host lattice is excited and then transfers this energy to the Eu^{3+}.

2.2 Absorption

Luminescent materials only emit radiation when the excitation energy is absorbed. Excitation spectra and absorption spectra typically show a strong correlation and both indicate that excitation energy can be absorbed either by the host lattice or by the activator itself. When high energy excitation such as fast electrons, gamma rays or X-rays and in our case, vacuum ultraviolet radiation is used, this always results in host lattice excitation. On the other hand, direct excitation of the activator is only possible with near-ultraviolet or visible radiation. The excitation spectra can tell us whether the host lattice or the activator absorbs the incident radiation.

The optical properties of a particular luminescent center in different host lattices are usually different because the immediate surroundings of such a center have been changed. Two main factors can be said to be responsible for the influence of the host lattice on the optical properties of a given activator in different host lattices. The first factor is covalency and the other is the crystal field. For higher covalency, the host lattice interactions between the electrons are reduced because they spread out over wider orbitals. Hence electronic transitions between different energy levels, which are determined by electron interaction shift to lower energy. A higher covalency also means that the constituent ions have a lower electronegativity difference between them so that the charge transfer transitions between these ions also shift to lower energy. For example, because YF_3 is more ionic than Y_2O_3, the charge transfer absorption band of Eu^{3+} shifts to a lower energy in the more covalent Y_2O_3.[8] Based on this, we can assume that Sr substitution for Ca would yield a more covalent compound and cause the excitation band

to move to a lower energy or higher wavelength. Conversely, alloying with Zn would move the excitation band to higher energies, which is would be consistent with our goal of shifting to lower excitation wavelengths. Ta has approximately the same electronegativity as Nb and so it is difficult to judge this effect in the metaniobate alloy system.

The effect of the crystal field effect of the host lattice on the optical properties of a luminescent ion is the second factor that influences the properties of an activator. The crystal field is the electric field imposed on the ion due to its surroundings. The strength of the crystal field then determines the spectral position of certain optical transitions. Different host lattices yield different crystal fields, which in turn yield different splittings such that the luminescent center can serve as a probe of the surroundings. Thus, the crystal field is responsible for the splitting of certain optical transitions and these observed splittings yield site symmetry.

One visible effect of the host lattice is the inhomogeneous broadening of the spectra. In powders, for example, the external surface may be large and activator ions, such as Eu^{3+}, near the surface may experience a covalency and a crystal field that is different from the bulk. These ions therefore have their optical transitions at slightly different energies from those in the bulk, which causes the spectra to broaden. Point defects in the crystal structure also contribute to this broadening. This effect helps to explain why even though calcium metaniobate is highly crystalline, we see a broad host absorption band. This broad band is also due to the vibrational overlap that occurs as a result of the interaction between the optical center and the vibrations of its surroundings. Vibrational overlap with several levels results in a broader absorption band and the larger

the difference in chemical bonding between the excited state and the ground state, the broader the absorption band.[8] The excited state in the NbO_6 complex of $CaNb_2O_6$ consists of Nb^{5+} ions and the valence state consists of O^{2-} ions. The bond enthalpy of the Nb-O bond is 771.5 KJ/mol, which is much higher than the Nb-Nb bond enthalpy (510 KJ/mol), when compared to the Nb-C bond enthalpy and most other bond enthalpies with Nb. Thus, the vibrational overlap contribution to band broadening can also be accounted for in $CaNb_2O_6$.

2.3 Emission

Emission can be defined as a radiative return to the ground state. Such a radiative return can occur when the absorption and emission processes occur in the same luminescent ion or center, or it can occur as a result of the influence of the host lattice on the emission transitions.

Typically, there is little or no emission during the relaxation process. The system can then return to the ground state upon the emission of radiation. This emission occurs spontaneously in the absence of a radiation field, while absorption can only occur in the presence of a radiation field. Emission in the presence of a radiation field is known as stimulated emission, but this process is not within the scope of this thesis. After emission, the luminescent center reaches a high vibrational level of the ground state, from which it relaxes to the lowest vibrational level of the ground state. The energy difference between the maximum of the excitation band and that of the emission band is known as the Stokes' shift. The larger the vibrational overlap, the larger the Stokes' shift and the broader the optical bands.

Energy transfer can occur between a pair of dissimilar luminescent centers or between identical luminescent centers. The case of dissimilar luminescent centers involves two centers: a sensitzer S and an activator A separated in a solid by a distance R, where R is assumed to be so short that S and A have a non-vanishing interaction with one another. This means that if S is in an excited state while A is in the ground state, then the relaxed excited state of S may transfer its energy to A. In this case, resonance has to be satisfied, that is, the energy differences between the ground and excited states have to be

equal and a suitable interaction has to exist for energy transfer to occur. This interaction can be an exchange interaction where there is a wave function overlap or an electric or magnetic multipolar interaction.[8]

Energy transfer between identical luminescent centers results in the phenomenon of concentration quenching of luminescence and a weak-coupling scheme or strong-coupling scheme can be applied to these centers. A typical case of stronger coupling is well-known in groups like tungstates and vanadates, which are oxidic anions with a central metal ion which has no d electrons, e.g. WO_4^{2-}, WO_6^{6-}, VO_4^{3-} and MoO_4^{2-}. Because the Stokes' shift of their emission is usually very large (~16000 cm^{-1}), energy migration is completely hampered, even at room temperature, e.g. in $CaWO_4$. In other cases such as YVO_4, thermally activated energy migration occurs and the Stokes' shift is much smaller (~10,000 cm^{-1}). The luminescent groups in WO_4^2 and NbO_4^{3-} have been proven to be isolated luminescent centers in spite of the short distance to their nearest neighbors[8]. The nature of the luminescent species determines the strength of the electron lattice coupling, for example, in the weak coupling case, the zero phonon line dominates and we see narrow peaks as in an Eu^{3+} emission. The coupling can be intermediate, in which case there is a gradual progression in the symmetrical stretching mode and where there is a broad band, this is an indication of strong coupling such as in $CaNb_2O_6$.

Transition metal ion complexes with a formally empty d shell typically show intense broad-band emission with a large Stokes shift on the order of 10 000 cm^{-1}- 20 000 cm^{-1}. Examples are VO_4^{3-}, NbO_6^{7-}, WO_4^{2-} and WO_6^{6-}. In the excited state, the electronic charge has moved from the oxygen ligands to the central metal ion and this is considered to be a charge transfer state. Actually, the amount of charge transfer is normally small but

a significant amount of electronic reorganization occurs whereby electrons are promoted from bonding orbitals in the ground state to antibonding orbitals in the excited state. This leads to a large value of ΔR in the configurational coordinate diagram, and broad spectral bands. [8] As can be expected, in $CaNb_2O_6$, where the electrons are promoted from O^{2-} bonding orbitals in the ground state, to the Nb^{5+} antibonding orbitals in the excited state, consequently the Stokes shift is large and the spectal bands are broad. In addition, the complexes with lighter metal ions, such as $Mg_4Nb_2O_9$, YVO_4, $CaWO_4$ and probably $CaNb_2O_6$, show long decay times as it has been proven that the emitting state in such compounds is a spin triplet.[9]

2.4 Photoluminescence

As has been defined earlier, luminescence occurs when some form of energy excites solids and this energy is released in the form of photons. When this solid is excited by short-wavelength light (usually UV radiation), the phenomenon is known as photoluminescence.

Photoluminescence can be classified as either intrinsic or extrinsic luminescence.

1. Intrinsic luminescence: As the name implies, intrinsic luminescence refers to a situation in which the luminescence comes from within a pure material or crystal. It may be grouped into three categories:

a.) Band-to-Band Luminescence:

This kind of luminescence occurs due to the recombination of an electron in the conduction band with a hole in the valence band, producing a band-to-band transition. This type of luminescence process can only be observed in very pure materials at relatively high temp-eratures, but is transformed into exciton luminescence at low temperatures. Examples of such materials are Si, Ge and some IIIb – Vb compounds such as GaAs.[11] The luminescence of $CaNb_2O_6$ under investigation in this study falls best into this category as well.

b.) Exciton Luminescence:

An exciton is a bound electron-hole pair in which an excited electron is interacting with a hole. As the exciton moves through the crystal, is carries some energy

and the electron and hole recombine to produce luminescence. There are two kinds of excitons. The Wannier exciton is composed of an electron in the conduction band and a hole in the valence band bound together by the coulomb interaction and is found primarily in IIIb – Vb and IIb – VIb inorganic semiconductors. The Frenkel exciton exists when the expanse of the electron and hole wavefunctions is smaller than the lattice constant and can be found in organic molecular crystals such as anthracene, inorganic complex salts such as tungstates and vanadates, and in uranyl salts.[11]

c.) Cross-Luminescence:

Cross –luminescence is produced when an electron in the valence band recombines with a hole created in the outermost core band. This kind of luminescence is typically observed in alkali and alkaline-earth halides and double halides.

2. Extrinsic Luminescence:

Extrinsic luminescence refers to luminescence caused by intentionally incorporating impurities or defects into a phosphor. In ionic crystals and semiconductors, it may be unlocalized or localized. It is unlocalized when the free electrons in the conduction band and free holes in the valence band of the host lattice also participate in the luminescence. On the other hand, the localized type occurs when the excitation and emission process of the luminescence are constrained within a localized luminescent center.

2.5 Crystal Structure

As has been discussed earlier, the present work began by investigating the pyroniobates ($M_2Nb_2O_7$) and pyrotantalates ($M_2Ta_2O_7$) as a possible alternative phosphor to the pyrophosphates. These materials have a structure composed of perovskite-type slabs with a thickness equal to twice the diagonal of a perovskite cube. The slabs are made up of NbO_6 or TaO_6 octahedra connected by sharing corners. The metal cations, M^{2+} are Ca^{2+}, Sr^{2+} and Ba^{2+}. Figure 2.2 below shows two successive ideal $Ca_2Nb_2O_7$ perovskite slabs in a projection down [010]. Successive slabs parallel to (100) are positioned so that one is shifted relative to another by c/4 or one-half of a perovskite cube edge. There are no direct links between NbO_6 octahedra in successive slabs. Because of the distortions in the orthorhombic structure of the $Ca_2Nb_2O_7$, the symmetry is actually reduced to a monoclinic structure. However, it is very nearly orthorhombic with a space group of $Cmc2_1$. $Ca_2Nb_2O_7$ and $Sr_2Nb_2O_7$ are believed to be isostructural with one another.[22]

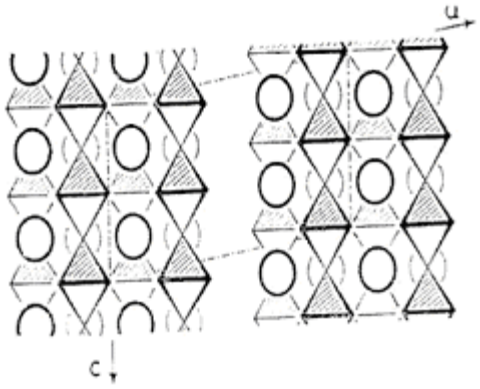

Figure 2.2. Structure of $Ca_2Nb_2O_7$ showing projection down [010] showing two successive slabs of $Ca_2Nb_2O_7$ parallel to (100). Slabs are drawn in their idealized perovskite form. The Ca ions and NbO_6 octahedra in light and heavy outline lie at y = _ and y = _ respectively. Distortions from this idealized structure are listed in the text. The broken lines and arrows show the projection of the true monoclinic unit cell.

Because it had been reported that $Ca_2Nb_2O_7$ is only luminescent at temperatures less than 100 K, the luminescence of a mixed phase of $CaNb_2O_6$ and $Ca_2Nb_2O_7$ at room temperature was attributed to $CaNb_2O_6$ upon synthesizing its single phase. The crystal structure of $CaNb_2O_6$ consists of calcium and niobium atoms surrounded by oxygen atoms in a polyhedral arrangement as shown in Figure 2.3. Each niobium octahedron shares two edges with adjoining niobium octahedra through the solid, which are linked to each other along their shortest edges. The chains of niobium octahedra, oriented along the c axis, are connected to each other through the calcium atoms, which forms a distorted irregular cuboid of oxygen atoms about the calcium atom.[2]

This structure is very similar to the columbite structure and the mineral known as fersmite contains about 89% $CaNb_2O_6$. The metaniobates (MNb_2O_6) and pyrotantalates (MTa_2O_6) of Ca, Ba, Mg, Sr, Zn, Cd and Pb are isostructural with one another and all have the columbite structure as reported by A. Wachtel[4].

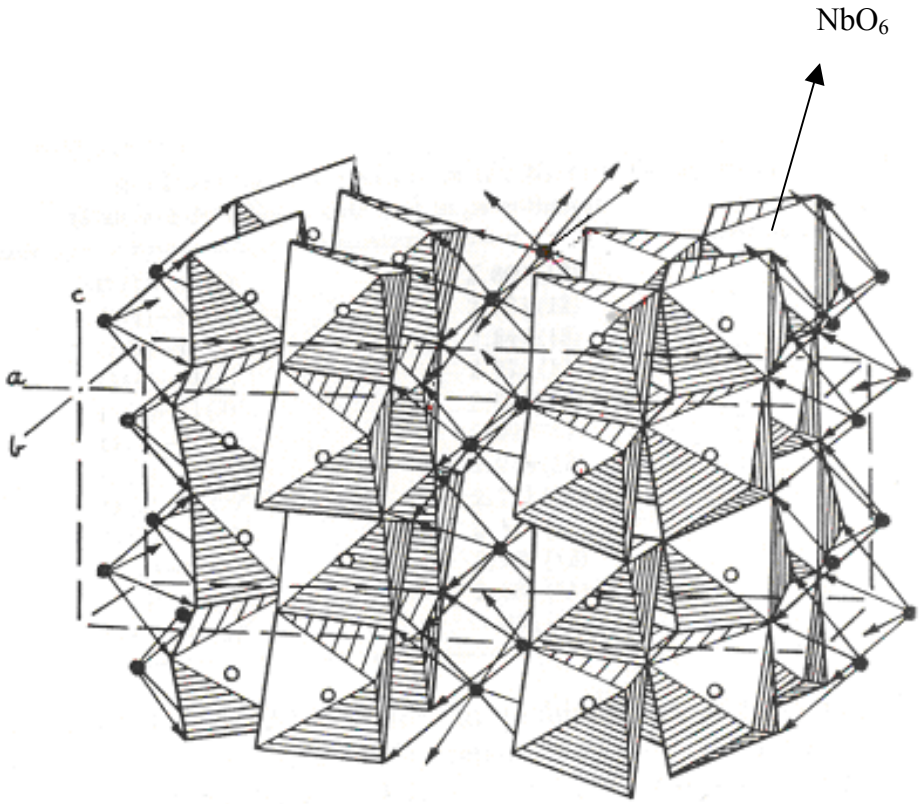

Figure 2.3. An artist's conception of the octahedral arrangement of oxygen atoms surrounding calcium and niobium atoms in the unit cell of calcium niobate; black circles are calcium; open circles are niobium. There are four calcium, eight niobium and twenty four oxygen atoms per unit cell.

2.6 Luminescence of Niobates and Tantalates

Tantalates and niobates with a perovskite structure have been known for several years as exhibiting ferroelectric and optoelectronic behavior. Some examples are $KNbO_3$ and $KTaO_3$ with a distorted perovskite structure, as well as $Sr_2Nb_2O_7$ and $Sr_2Ta_2O_7$ that have a structure of perovskite slabs. Although many niobates and tantalates are good luminescent materials that are increasingly used as x-ray phosphors, those with the perovskite structure do not even emit at room temperature. G. Blasse and L.H. Brixner compared these perovskite-like niobates and tantalates with titanates, which showed even worse luminescence properties.[1] They hypothesized that the poor spectroscopical properties in these niobates and tantalates is due to their considerable amount of electronic delocalization. The phosphors in the study were excited by wavelengths in the region between 260 nm to 450 nm. The emission bands were found at a maximum of 100 K in the case of $Sr_2Nb_2O_7$ and $Sr_2Ta_2O_7$ and in temperature dependent PL measurements, thermal quenching had occurred at about 50 % of the low temperature value.[1]

Compounds that contain a niobium-oxygen complex (NbO_6), as a more or less regular octahedron, belong to oxygenous octahedral niobates. It is generally considered that whatever the octahedron symmetry may be, the absorption edge of niobates is due to the charge transfer within this complex whose molecular orbitals form a valence band and a conduction band.[20] The basic luminescence mechanism, which has been described in detail by G. Blasse et al., is as follows.[6] The oxygenous octahedral niobates excited by light at the absorption edge region give a wide luminescent band whose minimum position for different niobates varies from 350 nm to 500 nm. This luminescence is

considered to be intrinsic and caused by a radiative transition from an excited state to the ground state within the NbO_6^{2-} complex. Under excitation, the electrons are excited from the most filled molecular orbitals localized at O^{2-} ions from the valence band, to one of the least filled molecular orbitals localized mainly at Nb^{5+} ions in the conduction band. The transition from the excited NbO_6^{2-} complex to the ground state is accompanied by a luminescence, which proves to be structurally sensitive, and allows the possibility of obtaining information on the structural variation and nonuniformities of a crystal lattice by means of luminescence measurements.[6]

Srivastava et al. discuss the low temperature luminescence properties of the perovskite-derived materials, in particular $Ba_5M_4O_{15}$ (M = Ta^{5+}, Nb^5).[2] The broad emission band for $Ba_5Ta_4O_{15}$ at 12 K showed a maximum at 455 nm while the excitation maximum was approximately 265 nm. The excitation and emission transitions are due to charge transfer transitions within the octahedral tantalate groups. At 100 K, the luminescence intensity decreased to 50 % of the low temperature value. Srivastava et al. explain that the excitation and emission maxima of the tantalates are always at energies higher than those of the corresponding niobates due to the higher 5^{th} ionization potential of tantalum as compared with niobium.[2] Also, in $Ba_5M_4O_{15}$ (M = Ta^{5+}, Nb^{5+}), the electronic delocalization of excitation energy through band formation is restricted, which is not the case in $Sr_2Ta_2O_7$ and $KTaO_3$. The luminescence of $(Ba_{0.98}K_{0.01}Eu_{0.01})_5$ was measured for λ_{exc} = 265 nm at three different temperatures. There was no change in intensity up to 30 K. However, above 30 K, the decrease in TaO_6 emission intensity is accompanied by an increase in Eu^{3+} emission intensity. This suggests that Eu^{3+} ions act as efficient acceptors for the TaO_6 excitation energy that becomes mobile for T > 30K.

Thus, the temperature-dependent luminescence quenching of pure $Ba_5Ta_4O_{15}$ was attributed to migration of the TaO_6 excitation energy to non-radiative quenching centers (defect centers) in the host lattice.[2]

A. Wachtel investigated the self-activated luminescence of M^{2+} niobates and tantalates in the 60's.[4] The metaniobates and pyroniobates of Ca, Ba, Mg, Sr, Zn, Cd and Pb were investigated. It was reported that the differences in the crystallography of the compounds seemed to be accompanied by significant differences in the luminescence exhibited. In particular, only the columbite structure of the metaniobates of Ca, Cd, Zn and Mg show a discernible room temperature luminescence of varying wavelengths in the blue spectral range. The luminescent efficiencies decrease with the decreasing size of the divalent cation thus decreasing from Ca^{2+} to Mg^{2+}. $CaTa_2O_6$ also shows a blue room temperature luminescence.[4] Visible emission was observed under excitation by a source of continuous UV, primarily at 254 nm. Due to the limitations of the equipment used, and the perceived lack of necessity of exciting at low wavelengths, no emission was investigated for excitation by wavelengths less than about 220 nm. The effect of the substitution of V for Nb in $CaNb_2O_6$ was also investigated and showed a shift in emission to longer wavelengths of green as well as a drastic reduction in brightness. The stronger luminescence of $CaNb_2O_6$ is attributed to an absorption edge shifted to shorter wavelengths whereas other niobates having a different structure absorb at longer wavelengths. This led to the conclusion that in the metaniobate compounds, the configuration of the ground and excited states of the Nb-O bond is favorable for luminescence in compounds with the columbite structure while the crossing over of the

ground and excited states in other structures may occur at lower energies, which also leads to low temperature quenching.[4]

The possibility of incorporating europium into $CaNb_2O_6$ for use as an inexpensive red lamp phosphor was investigated by Van der Voort et al., who also concluded that only the method of using appropriate associates or charge compensating species such as Na or K in the host lattice could satisfy the requirements of highly efficient Eu^{3+} emission.[5] No reduction of Eu^{3+} to Eu^{2+} to produce a blue emission was reported.

A comparison of the luminescence of $CaNb_2O_6$ and $CdNb_2O_6$ materials investigated by Blasse and van Leur shows that these materials have the columbite structure as well as emit intrinsically in the blue spectral range.[6] $YNbO_4$ and some other phosphors that have the fergusonite structure also show intrinsic blue emission and have been shown as good hosts for activation by other rare earths. While lanthanide host/ lanthanide activated phosphors are very efficient, this leads to a very expensive phosphor and is a major reason why much of the research is geared towards non-lanthanide host lattices[5]. The energy in compounds such as $YNbO_4$ is transferred efficiently from the host to the activator, producing primarily a Eu^{3+} emission. However, since a similar role had not been reported for calcium or cadmium metaniobates, W.A. McAllister investigated the luminescence, solid solutions and rare earth activation of these materials.[7] All the phosphors in the solid solution series $Ca_{1-x}Cd_xNb_2O_6$ showed a broad emission band at 470 nm for 285 nm excitation. Incorporation of Ln with Na as a charge compensating species into the solid solution led to considerable host emission whereas the incorporation of europium showed only the characteristic red emission. The cadmium-rich members were found to be superior in the study and the luminescence mechanism was explained as

follows. In niobates, the excitation is due to the transfer of an electron from one of the highest filled molecular orbitals on an adjacent oxygen (O^{2-}) to one of the lowest unfilled orbitals located on the Nb^{5+} ion.[6] Since all the $Ca_{1-x}Cd_xNb_2O_6$ phosphors have the columbite structure, the superiority of the cadmium rich materials was associated with the differences in the divalent ions. The three calcium 3p orbitals and five cadmium 4d orbitals differ in their directional characteristics even though their orbital radii are similar. Because the site symmetry is poorly defined in the case of cadmium, it may overlap with the adjacent oxygen ions resulting in the delocalization of the metal d electrons to the oxygens, which are in turn coupled to the niobium metal ions. The presence of these cadmium d electrons enables them to participate in the O^{2-} to Nb^{5+} charge transfer, which enhances the luminescence intensity. In contrast, the calcium 3p orbitals apparently do not participate in this electron sharing to as great and extent as the cadmium 4d orbitals. Blasse et al. also propose that the presence of Cd^{2+} ($4d^{10}$) ions favor the delocalization of the electrons belonging to the niobate group relative to that of Ca^{2+} $[Ar]4s^2$. Because the Stokes shift decreases and the excitation maximum shifts to lower energy from $CaNb_2O_6$ to $CdNb_2O_6$, they ascribe the 460 nm niobate emission of $CaNb_2O_6$ to self-trapped excitons on the niobate groups which are not mobile below room temperature. A similar explanation was given for the 420 nm emission of $CdNb_2O_6$ but the self-trapped excitons are mobile above 100 K.[5]

The structural and luminescent properties of the system of solid solutions formed by $ScNbO_4$ and $ScTaO_4$ have been investigated by L.H. Brixner.[8] It was reported that $ScNbO_4$ was slightly more efficient than $ScTaO_4$ when excited by 254 nm. However, the best quantum yields were observed for lower fractions of Nb with the maximum being at

about 0.2 moles of Nb and total concentration quenching never occurring in the system. $ScTaO_4$ was found to be an inefficient host for the rare earth ions Eu^{3+} and Tb^{3+} but can act as a host for efficient broadband Nb^{5+} emission.[8]

2.7 Solid State Synthesis

Two different powders A and B will only react if they are in close proximity and when they are mixed and heated together intimately. For this reason, solid state reactions require that there be a high degree of dispersion and mixing between the powders. When two reactants A and B react, a phase boundary is formed at the A – AB interface and another at the B – AB interface. Thus, each reactant has to diffuse through the AB phase in order to react. The overall solid state reaction is therefore dependent upon the rate of diffusion of the two reacting species. In addition, the rate of reaction, r, is usually analogous to the rates of solid state nucleation which are given by

$r = 1/V \ (dn_i/dt)$ for homogeneous nucleation

$r = 1/V \ \ (dV_t/dt)$ for heterogeneous nucleation

where n_i is initial moles, V_t is the volume at a given time, t, and V is the volume of the final product.

Diffusion-limited reactions are slow, so a combination of carbonate, phosphate or silicate sources and simple oxides can be chosen to overcome this limitation. This is because it is known that reactions between refractory oxides that are controlled by

diffusion result in mixtures of compounds, a situation we are trying to avoid. Using carbonate sources leads to an initial decomposition reaction as follows:

$$CaCO_{3\,(s)} \rightarrow CaO_{\,(s)} + CO_{2\,(g)} \quad (1)$$

The atomic-size CaO particles then react with Nb_2O_5 to produce $CaNb_2O_6$. Thus

$$CaO_{\,(s)} + Nb_2O_{5\,(s)} \rightarrow CaNb_2O_{6\,(s)} \quad (2)$$

The overall synthesis reaction is as follows

$$CaCO_{3\,(s)} + Nb_2O_{5\,(s)} \rightarrow CaNb_2O_{6\,(s)} + CO_{2\,(g)} \quad (3)$$

The reason why this reaction is very fast is that CaO, BaO, SrO, MgO, MnO and ZnO are produced in the form of very small particles which react quickly with Nb_2O_5 or Ta_2O_5 to form $CaNb_2O_6$ or $Ca(Nb,Ta)_2O_6$. Indeed, the rate of reaction is proportional to the number of nuclei produced per unit volume.[12] Thus, in order to increase the solid state reaction rates, a decomposition reaction is used to supply the reacting species such as CaO in atomic proportions so that it reacts nearly as fast as the CaO is formed and the number of nuclei produced per unit volume is greatly increased. Also, because CaO, BaO, SrO and the other simple oxides have a very large surface area, the solid state reaction is not diffusion limited.[12]

The reaction of solids, particularly when nucleation is present occurs either by surface or volume nucleation. There are usually two stages during which solids react: nucleation, and then growth of the nuclei. The decomposition reaction of $CaCO_3$, which occurs in the formation of $CaNb_2O_6$ is an example of volume nucleation. This reaction is relatively slow compared to one which involves a gas or liquid nucleation of the solid.

CHAPTER III

EXPERIMENTAL PROCEDURE

Section 3.1 Synthesis Procedure

The phosphors in this study were synthesized by a solid state reaction using a wet milling process. Carbonate sources were used for the 2+ cations, while oxide sources where used for Nb and Ta to increase the rates of diffusion-controlled reactions, which are typically slow. In the preparation of $CaNb_2O_6$, for example, the stoichiometric compositions of $CaCO_3$ and Nb_2O_5 were measured and the powders were ground in a crucible for approximately 5 minutes. The powders were then placed in polyethylene bottles and ethanol and Zirconia balls were added. These materials were ball milled for approximately 4 hours, which was found to be sufficient time to allow the powders to react intimately. The balls were removed and the mixture of ethanol and phosphor was placed in a centrifuge to remove the ethanol. The wet powders were then dried in a drying oven at 82 °C for 10 hours. A first firing was performed at 800 °C for two hours in order for the decomposition reaction $CaCO_3 \rightarrow CaO + CO_2$ to occur. The heating rate and cooling rate were set at 4 °C/min respectively for all firings. The samples were ground again after the first firing to ensure the homogeneity of the powders. A second firing was then performed at 1200 °C for two hours, as that was found to be the optimum temperature for the formation of the pure $CaNb_2O_6$ compound as well as for the highest degree of crystallinity. The reaction achieved in the second firing was as follows: $CaO_{(s)} + Nb_2O_{5\,(s)} \rightarrow CaNb_2O_{6\,(s)}$. The powders were finally ground in order to prepare the samples for X-ray diffraction, photoluminescence and SEM measurements.

Section 3.2 Optimization of Synthesis Parameters

A preliminary study was carried out to optimize the stoichiometry and firing conditions of $CaNb_2O_6$. All samples were prepared with the stoichiometric formula and were undoped in the initial investigation as these phosphors exhibit a self-activated luminescence. Five variations of the stoichiometry and five second firing temperatures were then performed, which led to a sample space of 25 samples shown in Table 3.1 below. Table 3.1 also shows the purity of the phase determined by X-ray diffraction for the different firing temperatures and stoichiometric variations.

Table 3.1 Optimization of Stoichiometry and Firing temperature.

	1000 °C	1100 °C	1200 °C	1300 °C	1400 °C
Stoichiometric	Mixed Phase	Mixed Phase	Pure Phase	Pure Phase	--
10 % Xs. Ca	Mixed Phase	Mixed Phase	Pure Phase	Pure Phase	No match
20% Xs. Ca	Mixed Phase	Pure Phase	Pure Phase	Pure Phase	No match
10% Xs. Nb	Mixed Phase	Mixed Phase	Pure Phase	Pure Phase	--
20% Xs. Nb	Mixed Phase	Mixed Phase	Mixed Phase	Pure Phase	--

Section 3.3 X-ray Diffraction

X-ray diffraction was used to identify the phases, determine the crystallinity of the structure and to detect the degree of solubility or discontinuities in the solid solutions. The diffractometer used was a Phillips PW 1800 model, equipped with a cooper X-ray tube. The measurements were taken at a generator tension of 40 KV and a current of 20 mA using Cu □□ rays. A 2_ step size of 0.02 and continuous scanning at an angular rate of 0.008 °/s at a time per step of 0.5 were used to obtain the diffraction spectra from 2_ angles of 20° to 50°. The X-ray diffraction spectra show the intensities of the diffraction peaks as a function of the detecting angle 2□. The interplanar spacings, d, corresponding to the peaks are calculated from Bragg's diffraction law, n□ = 2dsin□, in the first order.[15] Miller indices were then assigned to the reflection peaks in the diffraction pattern by comparing the data obtained from the samples to the X-ray diffraction data for pure compounds, which are published by the International Center for Diffraction Data (ICCD).

The interpretation of the powder patterns of alloys is based on the fact that each phase produces its own pattern independently of the presence or absence of other phases.[18] A continuous solid solution is generally of the substitutional type and varies in composition from a pure end-member, A to a pure end-member B, which must have the same structure. Therefore, because all alloys in such a solution have the same structure, their powder patterns appear quite similar, except that changes in composition shift the diffraction-line positions as the lattice parameter changes. More commonly, however, as in the metaniobate alloys, the terminal solutions A and B are only partially soluble in one another. Initial addition of A atoms into B sites produces a solid solution, which causes

the B lattice to expand or contract depending on the relative sizes of the A and B atoms. The lattice expands if the substituting atom A, is larger than the B atom and contracts if it is smaller. As a result of the size mismatch between the atoms, a solubility limit is reached such that further additions of one atom causes the precipitation of a third phase, which may be rich A-rich or B-rich (depending on which one is substituting), or an intermediate phase if it is not connected with either phase. The crystal structure of this intermediate solid solution is entirely different from that of either end member.[18]

Section 3.4 Photoluminescence Instrumentation

Photoluminescence spectroscopy has been accomplished through vacuum ultraviolet (VUV) excitation followed by a photon emission measurement. Excitation photons were produced with a Deuterium Lamp – Hamamatsu Model L1835, which is capable of efficient emission in the range from 115 nm to 400 nm. The light produced is then directed to a spherical mirror, which focuses the photon stream to the entrance slit of the vacuum monochromator – ARC Model VM-502. The selection of the excitation wavelength was achieved with a 1200 G/mm grating that is coated with Iridium, allowing it to be used in the far UV regime of the electromagnetic spectrum. The light coming from the entrance slit of the vacuum monochromator as a point source falls on the grating so that the full spectrum is achieved. The grating is rotated so that the wavelength is selected using an ARC SpectraDrive Model 748 which is computer controlled with LabView drivers. Photons with a specific wavelength are then focused to the entrance slit of the sample chamber. A Turbodyne pump was used to keep the spherical mirror housing, sample chamber and monochromator/grating under vacuum.

The samples are irradiated in a sample chamber with a four-specimen holder, each specimen having a 10 mm diameter by 1 mm thick cavity with MgF_2 cover plates. Photons with a specific wavelength originating at the entrance slit of the vacuum monochromator as a point source, strike the flat sample surface at an angle of 60º to the plane perpendicular to the central beam path. This wide angle i.e. greater than 45º, allows the excitation photons to interact with a thinner surface layer and produces a greater area from which emitted photons can be measured. The photoluminescence emission flows

out of the sample chamber as a wide beam through a glass window, which is confined and directed to the spectrometer through the use of collimating and focusing lenses. The focused light then passes through a filter which prevents any wavelengths less than 335 nm from entering the measurement system.

The emission wavelength selection was accomplished using a second 1200 G/mm grating housed inside the spectrometer. The photoluminescence emission originating from the entrance slit fills a collimating mirror with the full spectrum where it is reflected to the grating for wavelength selection. The photons of specific wavelengths are then passed to a focusing mirror which directs the beam to the side exit mirror, enabling it to escape through the exit slit. The total focal length of the spectrometer is 0.27 m. Photons originating from the spectrometer exit slit are focused through a photomultiplier tube (PMT) housing that contains a Hamamatsu End-On type PMT, by a vacuum sealed lens. The PMT is thermoelectrically cooled to significantly reduce the noise that would otherwise be produced by thermal electrons. All elements of the spectrometer were computer controlled using the Spectromax software including for photon counting. A schematic of the entire set up is shown in Figure 3.1.

Although the sample chamber is capable of holding four specimens, the first position, (1), is always occupied by a Sodium Salicylate standard with a peak emission at about 420 nm under 147 nm excitation. Thus, to ensure that a consistent photon count is achieved between measured samples, this position is monitored while optical adjustments are made.

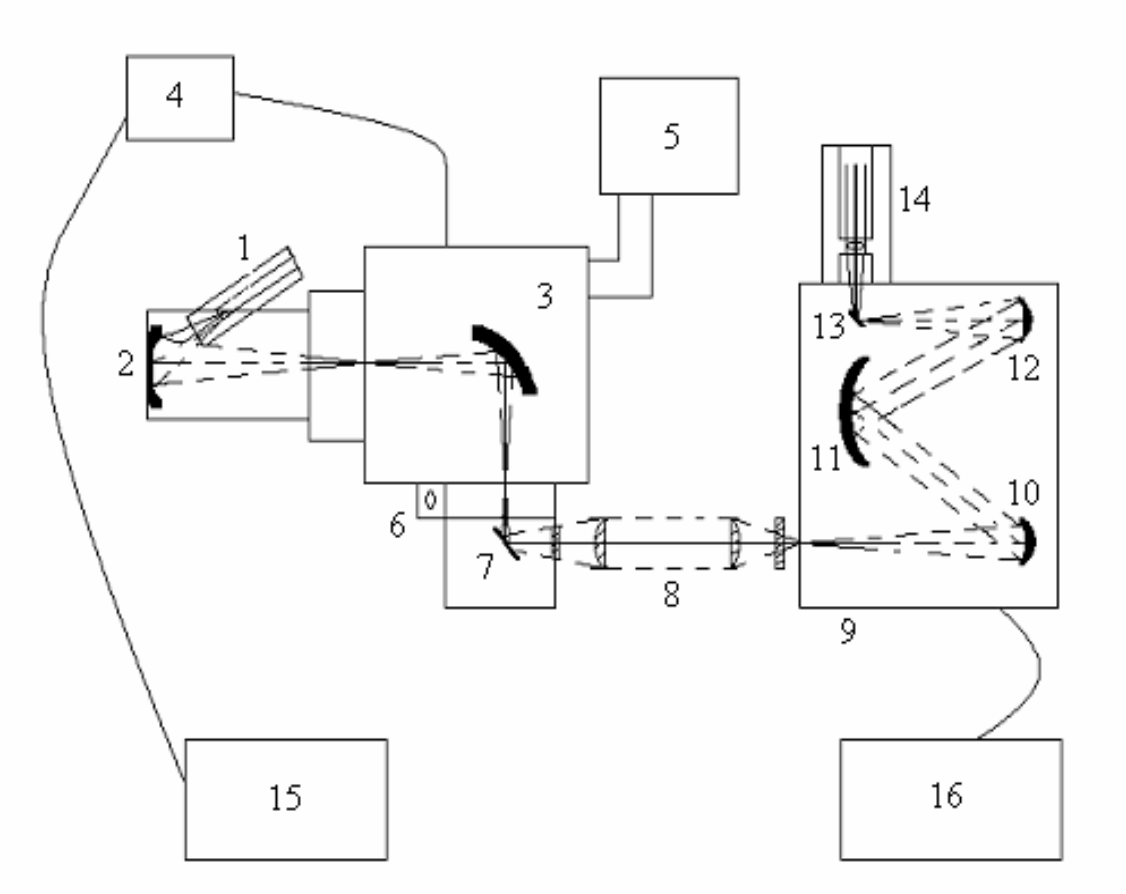

Figure 3.1 Arrangement of photoluminescence spectroscopy system.

1. Deuterium Lamp – Hamamatsu Model L1835 (150W)
2. Spherical Mirror
3. VUV Monochromator with Iridium Coated Grating (1200 G/mm) ARC Model VM-502
4. Monochromator Control-ARC SpectraDrive Model 748
5. TurboDyne Pump
6. Beam Monitor
7. Sample Chamber with (4) Specimen Holder
8. Collimating and Focusing Lenses followed by 335 nm Optical Filter
9. Spectrometer – ISA Model 270M (0.27 m focal length)
10. Collimating Mirror
11. Grating (1200 G/mm)
12. Focusing Mirror
13. Side Exit Mirror
14. Photomultiplier Tube Housing with Focusing Lens
15. Computer No.1 – controlling excitation wavelength
16. Computer No.2 – controlling spectrometer and PMT.

Section 3.5 Photoluminescence (PL) and Photoluminescence Excitation (PLE)

The photoluminescence spectrum (PL) is obtained by the selection of a single excitation wavelength, followed by the spectroscopic scanning of multiple emission wavelengths. A scan rate of 0.5 nm per step with an integration time of one second is used. Due to differences in the experimental conditions before the measurements, such as changes in the intensity of the reflected beam of the standard sample, PL patterns samples recorded at different times are corrected for the 1200 G/mm grating used in the spectrometer and factored with respect to the PL curve of the standard sample.

Photoluminescence excitation (PLE) measurements involve excitation by a range of wavelengths, while the wavelength of the emitted photons is fixed. Thus, the monitoring wavelength is selected as the peak position determined in the PL measurement, unless one is interested in collecting an excitation spectrum at another emission wavelength. As the spectrometer / PMT is commanded to count photons for a specified length of time while the excitation wavelengths are scanned, a time versus intensity plot is produced. The time must then be converted to wavelengths based on the excitation scan rate of 12 nm per minute that is typically used. However, because the Deuterium Lamp (Hamamatsu L1835) has an extremely high peak corresponding to significant photon production of 162 nm wavelength, the spectrum of the sample taken must also be adjusted relative to the intrinsic spectrum of the lamp. Thus, a quantum efficiency “relative” to that of the Sodium Salicylate standard is presented in a PLE spectrum.

Section 3.6 Scanning Electron Microscopy

The phosphors have been examined by scanning electron microscopy (SEM) using the LEO microscope to determine the particle morphology and estimate the particle size. In insulating specimens such as our phosphors samples, charging effects are often observed because the charges that are generated from the electron-specimen interactions cannot readily flow to the ground. This results in an accumulation of charge that causes the specimen to undergo a continually changing state of surface potential.[26] Voltage contrast then develops in which the potential distribution across the image becomes so large that it can overshadow the contrast of the true specimen features. [19,26] Thus, the samples are typically spin-coated with a thin layer of gold to avoid the charging effects, but because low voltage measurements were taken and due to the powerful detection capability of the LEO microscope, these effects were reduced and it was possible to get images showing well defined features even without the gold coating.

The sample grid was inserted and aligned horizontally inside the chamber but appeared vertical on the screen. The z-axis control was set to 20 mm and vacuum was drawn from the sample chamber. The accelerating voltage was then set at 3 kV, while the working distance used was 7 mm.

CHAPTER IV

RESULTS

4.1 Optimization of Stoichiometry and Firing Temperature

The optimum synthesis conditions for the fomation of the single phase of the compound showing the best emission were determined initially by XRD analysis. Single phases of $CaNb_2O_6$ were primarily obtained for firing temperatures of 1200 °C and 1300°C as shown in Table 3.1. Thus, a photoluminescence study of the samples fired at 1200 °C and 1300 °C was performed to try to conclusively determine the optimum synthesis conditions. The PL spectra comparing all the samples involved are shown in Figure 4.1.

This figure shows that the calcium metaniobate fired at 1200 °C using the stoichiometric compositions had the best emission. Subsequently, a PL analysis of the samples fired at 1200 °C was performed to verify the best composition stoichiometry.

Figure 4.2 shows that there is no specific order of PL intensities with respect to the starting compositions but the sample prepared with 10% excess $CaCO_3$ was the most intense, followed by 20% excess Nb_2O_5 and then the stoichiometric composition. However, in order to perform additional studies, it would be best to synthesize $CaNb_2O_6$ using the stoichiometric composition or a slight excess of $CaCO_3$ to prevent reactions with other compounds that could lead to the formation of an undesired material. The peak corresponding to the maximum intensity is at 464.5 nm for all compositions except for 10% excess $CaCO_3$, where there is a shift to 456.5 nm.

From the PLE spectra shown in Figure 4.3, the maximum excitation bands are at 209 nm for $CaNb_2O_6$ and 254 nm for 20% excess Nb_2O_5. In the samples prepared with the stoichiometric composition, 10% excess Nb_2O_5, 10% excess $CaCO_3$, and 20% excess $CaCO_3$ the maximum excitation band is at 260 nm with a gradual decrease to 148 nm. An increase in the relative quantum efficiency is then observed at lower wavelengths. However it can be seen clearly that there is some absorption at 172 nm and some at 147 nm as well, particularly for the 10% excess $CaCO_3$ composition, which also has a strong PL intensity for 147 nm excitation. Thus, if the excitation band can be shifted to lower wavelengths, then there would be much better absorption at 147 nm.

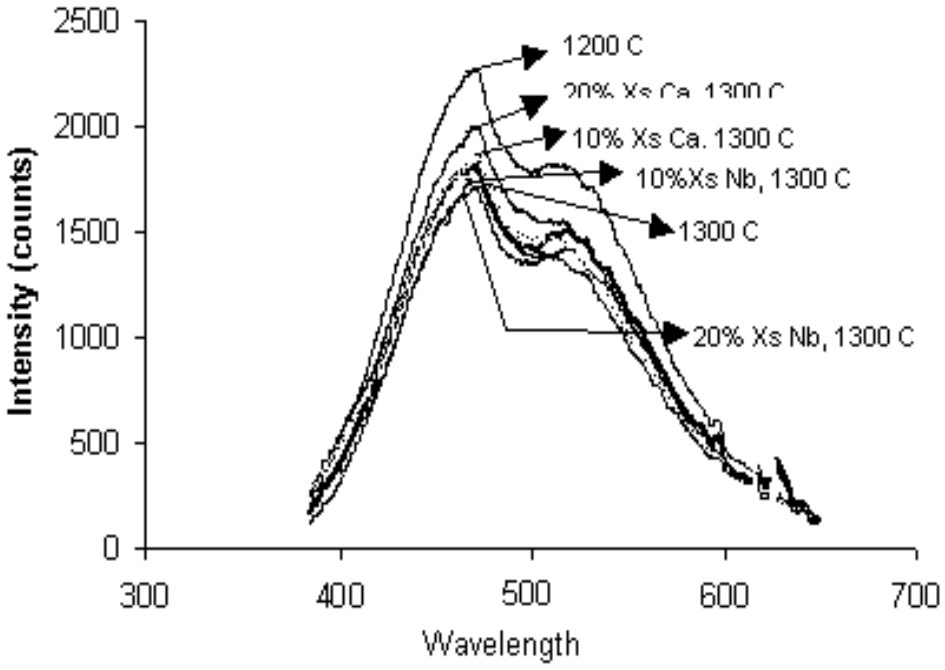

Figure 4.1 Photoluminescence of Various Compositions of $CaNb_2O_6$ Fired at 1300 °C and 1200 °C

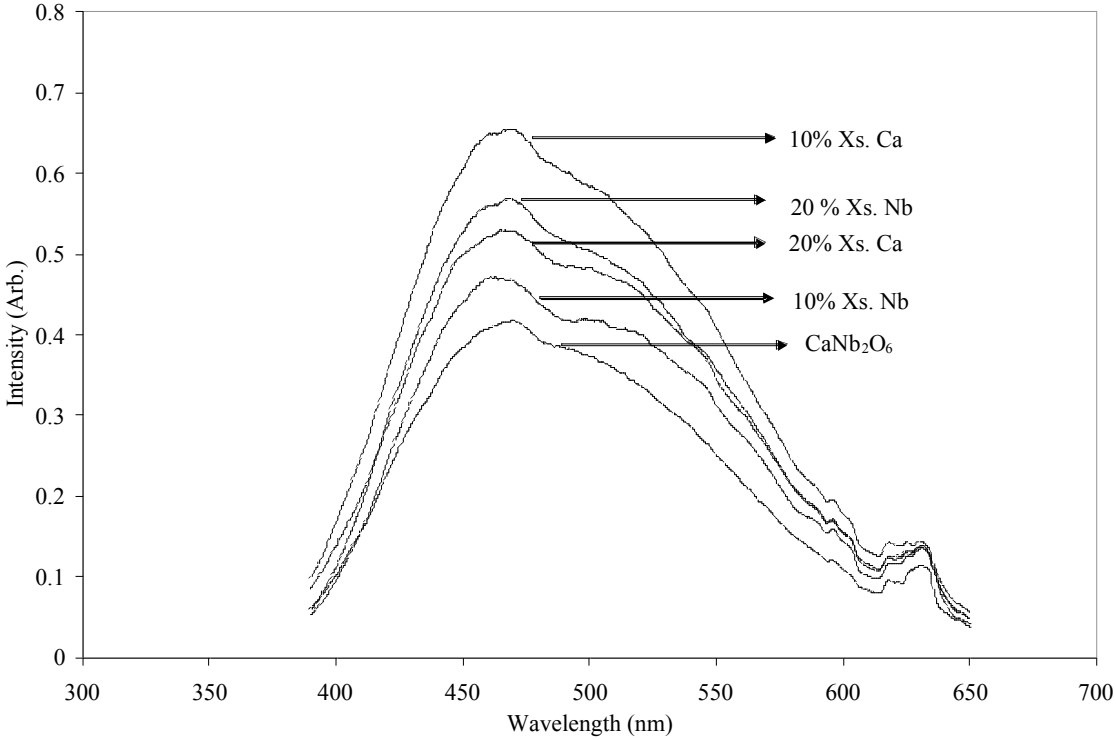

Figure 4.2 Photoluminescence of various compositions of $CaNb_2O_6$ fired at 1200 °C

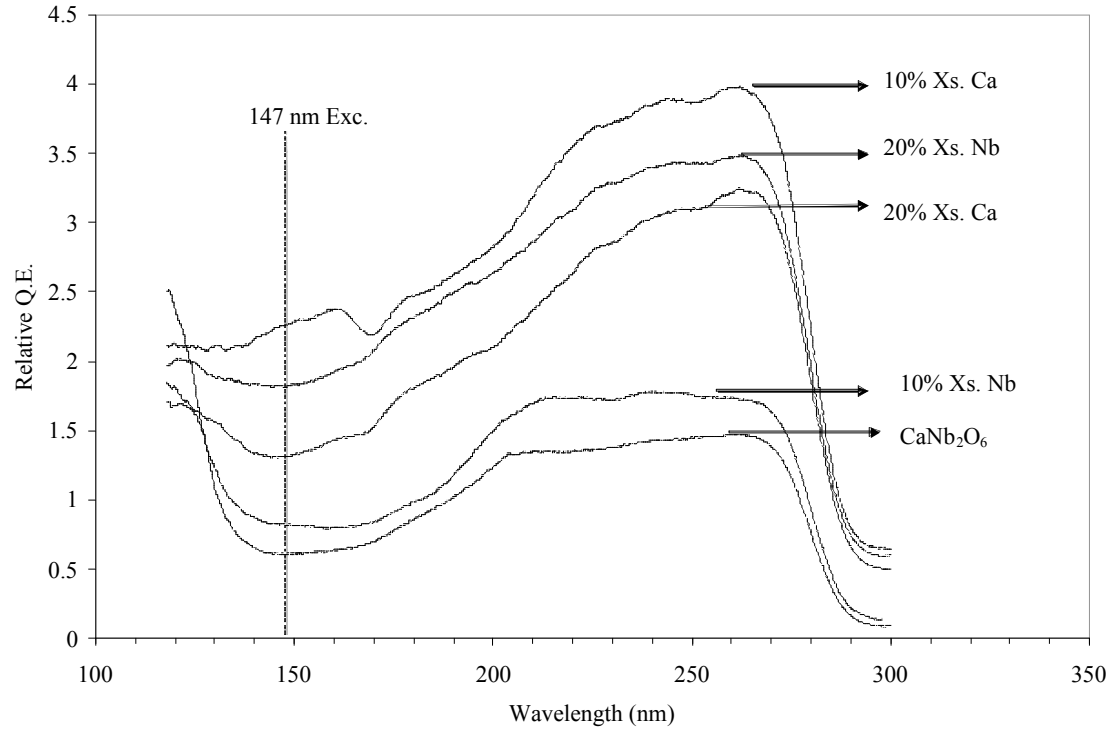

Figure 4.3 PLE of various compositions of $CaNb_2O_6$ at 1200 °C

4.2 Structure And Chemical Analysis

In order to affect the crystal structure and hence tune the chromaticity and emission intensity of $CaNb_2O_6$, alloys of Ca with other 2+ cations were made and Ta was substituted for Nb as shown in Table 4.1. The X-ray spectrum of calcium metaniobate in Figure 4.4 shows a good crystallinity with an intense and narrow primary peak.

Table 4.1 Synthesis of Solid Solutions

Composition	X	x	x	x	x	x	x	x	x	x	x
$Ca_{1-x}Sr_xNb_2O_6$	0	0.1	0.2	0.3	0.4	0.5					
$Ca_{1-x}Zn_xNb_2O_6$	0	0.1	0.2	0.3	0.4	0.5	0.6	0.7	0.8	0.9	1.0
$CaNb_{2(1-x)}Ta_{2x}O_6$	0	0.1	0.2	0.3	0.4	0.5	0.6	0.7	0.8	0.9	1.0
$Ca_{1-x}Ba_xNb_2O_6$	0	0.1	0.2	0.3							
$Ca_{1-x}Mg_xNb_2O_6$	0	0.1	0.2	0.3							

The XRD spectrum of pure calcium metaniobate is shown in Figure 4.2.1 below.

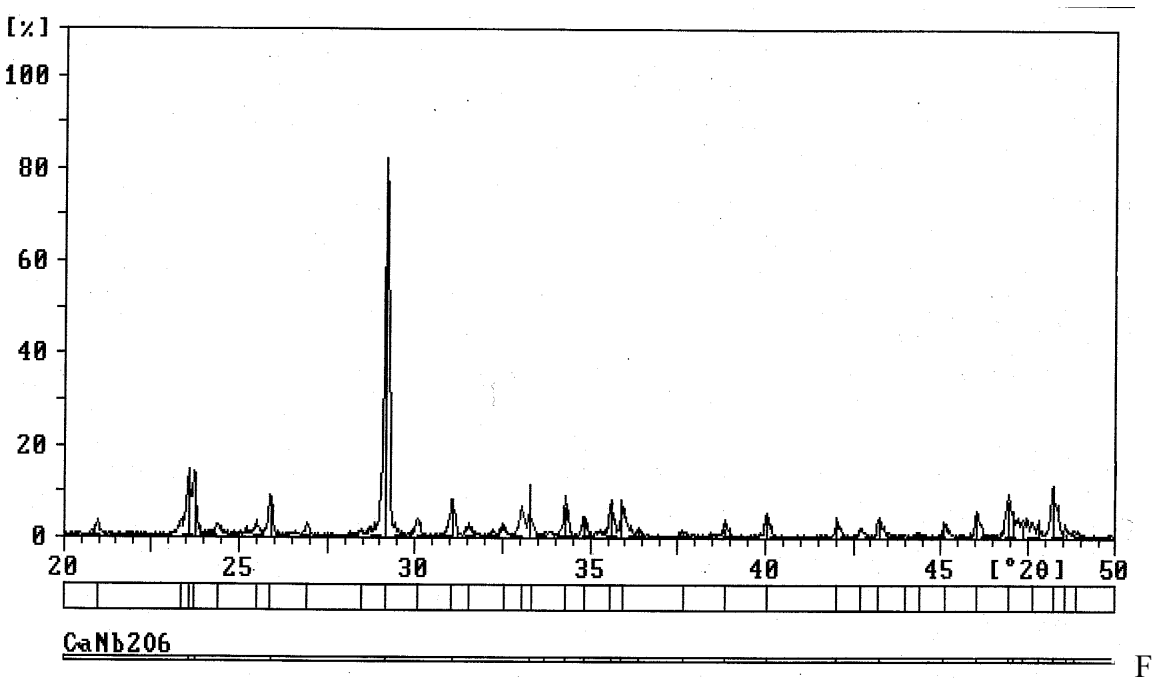

F

Figure 4.4 Calcium Metaniobate fired at 1200 °C. Blue luminescence.

4.2.1 X-Ray Diffraction of $Ca_{1-x}Sr_xNb_2O_6$

It can be observed from Figure 4.5 that the powder patterns of all the alloys are quite similar which indicates a continuous solid solution and that the columbite crystal structure remains the same for all the alloys synthesized. The intensity of the luminescent peak at a 2_ angle of 29° decreases systematically as Sr is substituted into the alloy.

Secondly, because Sr^{2+} (1.13 A°) is slightly larger than Ca^{2+} (0.99 A°), there is an expansion of the lattice surroundling the NbO_6^{2-} octahedron. However, because the difference in size is small (less than 15%), stresses that arise due to the ionic mismatch are not very significant.

Finally, small peak shifts to smaller 2_ angles are also observed, which are due to the change in composition as Sr is added into the alloy. By Bragg's Law (n_ = 2dsin _), decreasing values of _ correspond to an increase in the interplanar spacing d, which increases at least one lattice parameter and thus a lattice expansion in at least one direction. The interplanar spacing for the orthorhombic structure is given by $\frac{1}{d^2} = \frac{h^2}{a^2} + \frac{k^2}{b^2} + \frac{l^2}{c^2}$. More precise calculations are needed to show the relationship between the interplanar spacing d, and the cell volume but the explanation given above justifies using a larger alkali earth metal than Ca to expand the lattice thus increasing the crystal field imposed on the luminescent ion.

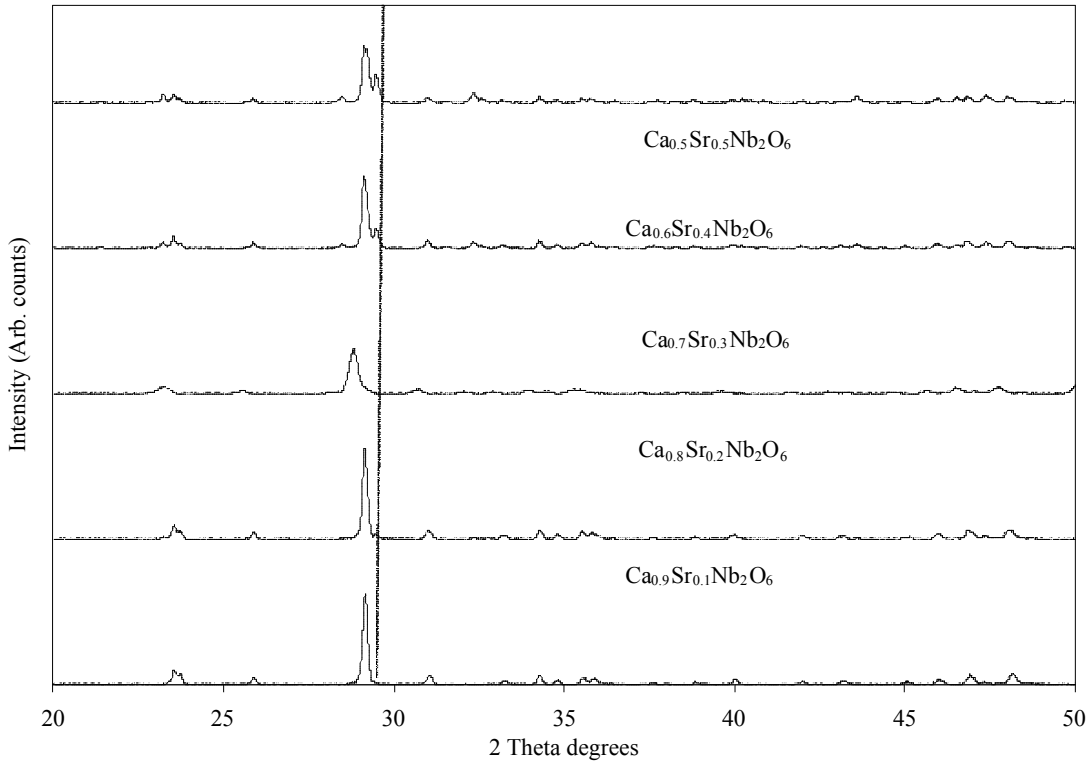

Figure 4.5. X-ray diffraction spectra of $Ca_{1-x}Sr_xNb_2O_6$ for x = 0.1 to x = 0.5.

4.2.2 X-Ray Diffraction of $Ca_{1-x}Zn_xNb_2O_6$

The substitutions of x = 0.1 and x = 0.2 in Figure 4.6 show x-ray spectra that are very similar to that of $CaNb_2O_6$. We then observe a change in the pattern from x = 0.3 to x = 0.4 and x = 0.5 in which there is a large decrease in ratio of the primary $CaNb_2O_6$ peak with respect to the dominant $ZnNb_2O_6$. Thus, the solid solution is continuous up to x = 0.2 after which there appears to be precipitation of an intermediate phase that results in a reduction of the primary peak intensity, which also corresponds to a decrease in the PL intensity will be shown.

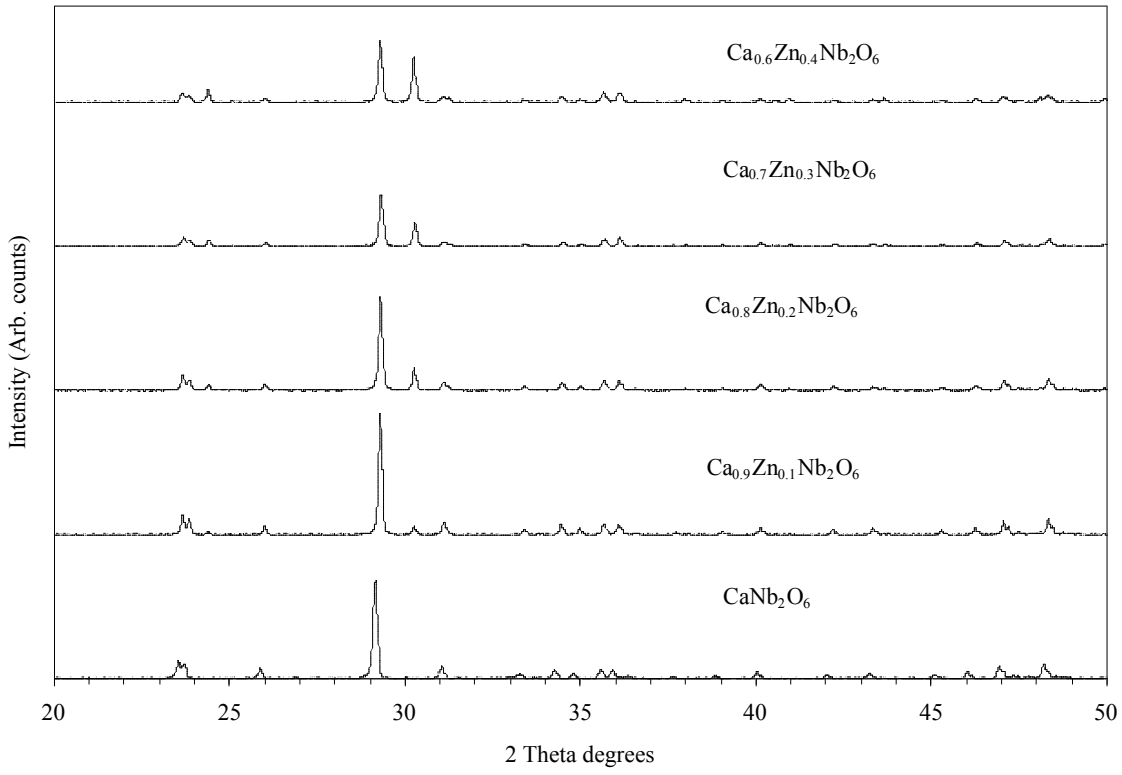

Figure 4.6. X-ray diffraction spectra of $Ca_{1-x}Zn_xNb_2O_6$ for x = 0 to x = 0.4.

4.2.3 X-Ray Diffraction of $CaNb_{2x}Ta_{2(1-x)}O_6$

Based on the XRD results of this alloy system, the columbite structure of $CaNb_2O_6$ changes for x=0.4 to x=0.8 to an intermediate phase known as rynersonite with the formula, $Ca(Ta,Nb)_2O_6$. The terminal solutions are both columbite but rynersonite is reported to be in the class of columbite-group-materials (CGM) and so the solid solution can be considered to be continous. The columbite structure is responsible for efficient luminescence in metaniobate compounds and a minor change in structure is not expected to produce a dramatic change in the emission for consecutive points in the alloy system. In addition, there are slight shifts in the primary peak to the right, which simply indicate a change in the compostion as shown in Figure 4.7.

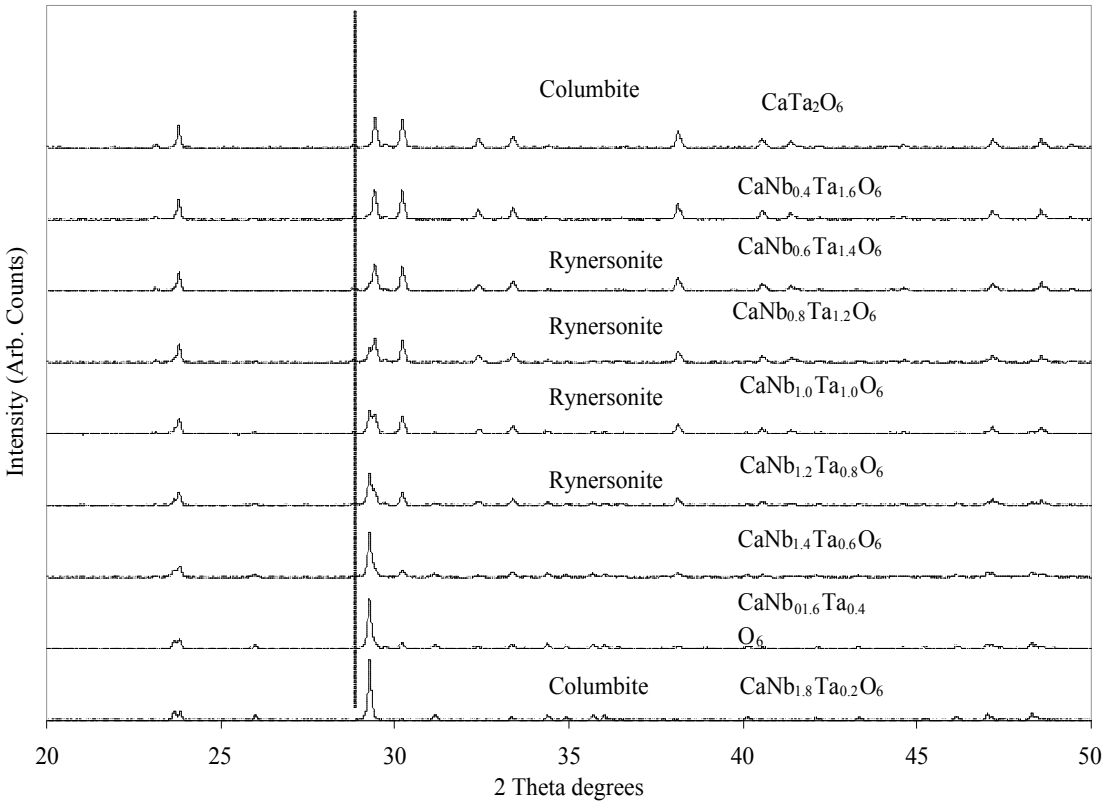

Figure 4.7. X-ray diffraction spectra of $CaNb_{2(1-x)}Ta_{2x}O_6$ for x = 0.1 to x = 1.

4.2.4 X-Ray Diffraction of $Ca_{1-x}Ba_xNb_2O_6$

The substitutions of x = 0.1 and x = 0.2 in Figure 4.8 show x-ray spectra that are very similar to that of $CaNb_2O_6$. We then observe a change in the pattern at x = 0.3 in which there is a drastic decrease in intensity of the primary $CaNb_2O_6$ peak. Thus, the solid solution is continuous up to x = 0.2 after which there appears to be precipitation of an intermediate phase that results in a reduction of the primary peak intensity, which also corresponds to a decrease in the emission intensity. Also, at x = 0.3, the primary peak shifts markedly to the right of the peaks of x = 0.1 and x = 0.2.

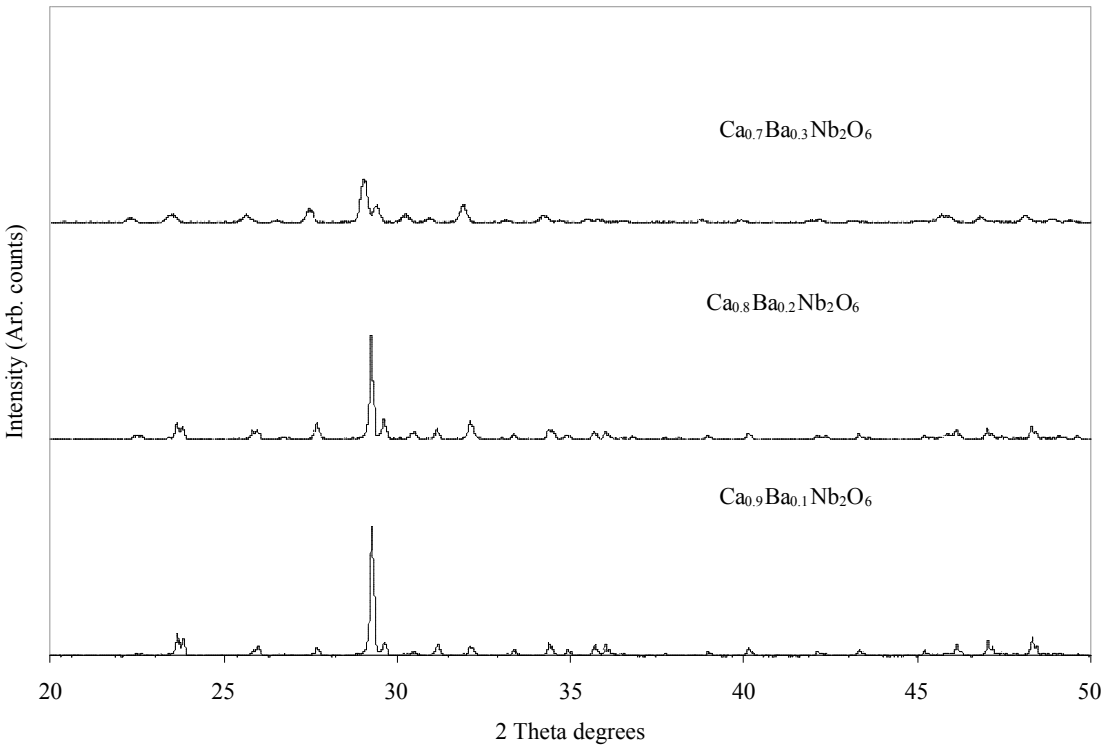

Figure 4.8. X-ray diffraction spectra of $Ca_{1-x}Ba_xNb_2O_6$ for x = 0.1 to x = 0.3.

4.2.5 X-Ray Diffraction of $Ca_{1-x}Mg_xNb_2O_6$

In this alloy, substituting x = 0.1 and x = 0.2 and x = 0.3 as in Figure 4.9 show x-ray spectra that are very similar to that of $CaNb_2O_6$. The reduction in the intensity of the primary peak is systematic and there is no noticeable change in the peak position. Thus, the solid solution appears to be continuous at least up to x = 0.3. However, because Mg is smaller than Ca the contraction of the lattice causes a decrease in the emission of the intrinsic $CaNb_2O_6$ as will be shown conclusively in the next section.

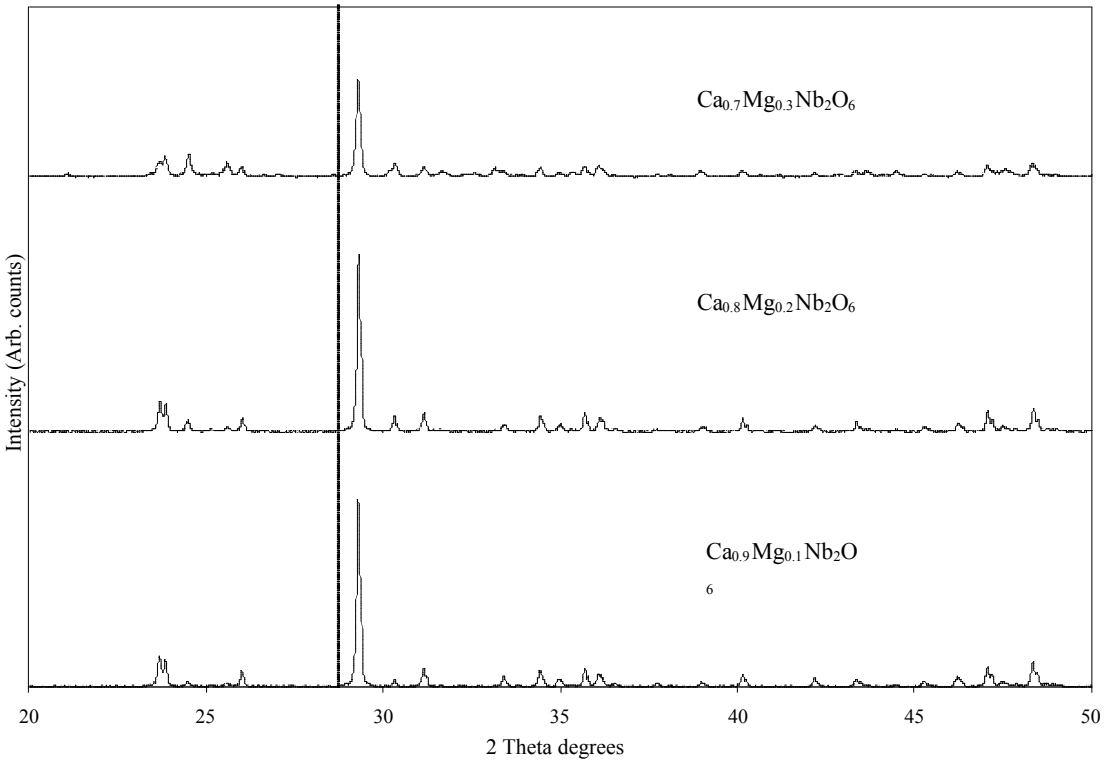

Figure 4.9. X-ray diffraction spectra of $Ca_{1-x}Mg_xNb_2O_6$ for x = 0.1 to x = 0.3

4.3 Optical Characterization

The optical characterization of the alloys of $CaNb_2O_6$ was done by photoluminescence and photoluminescence excitation measurements. These measurements show a change in the emission intensity and the excitation maxima as a function of alloying in order to allow us to correlate this data with the structural and chemical data from XRD.

4.3.1. PL and PLE of $Ca_{1-x}Sr_xNb_2O_6$

The alloy system $Ca_{1-x}Sr_xNb_2O_6$ for x values of 0, 0.1, 0.2, 0.3, 0.4 and 0.5 was investigated. The crystal structure of $CaNb_2O_6$ consists of an NbO_6^{2-} octahedron surrounded by an irregular cuboid of Ca atoms. Because Sr is a larger ion than Ca, its substitution causes a lattice expansion, which increases the strength of the crystal field that the luminescent center experiences. The spectra in Figure 4.6 show that the most intense emission in the $Ca_{1-x}Sr_xNb_2O_6$ comes from x = 0.2, followed by x = 0.1 and then x = 0. The intensity then decreases for x = 0.3 to x = 0.4 and x = 0.5. Based on these results, a 20 mol % substitution of Sr into Ca sites causes the largest expansion of the lattice that causes the strongest crystal field around the NbO_6^{2-} octahedron, which allows for the blue emission. This increases the emission intensity of pure $CaNb_2O_6$ dramatically by almost twice the value or about 95%. A slightly lower effect is observed for a 10 mol % addition of Sr, which results in a 65% increase in the intrinsic emission. However, a

decrease in the intrinsic $CaNb_2O_6$ intensity by 15% is observed for x = 0.3 and decreasing further for x = 0.4 and x= 0.5 as the alloy approaches a non-luminescent $SrNb_2O_6$ phase and this is consistent with the PL results shown in figure 4.10. This is also consistent with a discontinuity in the solid solution as shown in the XRD spectra of figure 4.4 as expected, due to the highly sensitive dependence of the luminescence on the structure in metaniobate compounds. The positions of the emission peaks increase with additions of Sr from 460 nm at x = 0.1 to 464.5 nm at x = 0.2 and 470 nm at x = 0.3.

The PLE spectra in Figure 4.11 indicate only host lattice excitation and show that the quantum efficiency is best for smaller mole fractions of Sr, the highest being x = 0.1 followed by x = 0.3 and x = 0.2. The lowest efficiencies are at x = 0.4 and x = 0.5. Combining these with the PL spectra where the differences in intensities are more dramatic, we find that the absorption and the emission increase for lower concentrations of Sr but increases for higher concentrations as the system approaches the non-luminescent Sr end member.

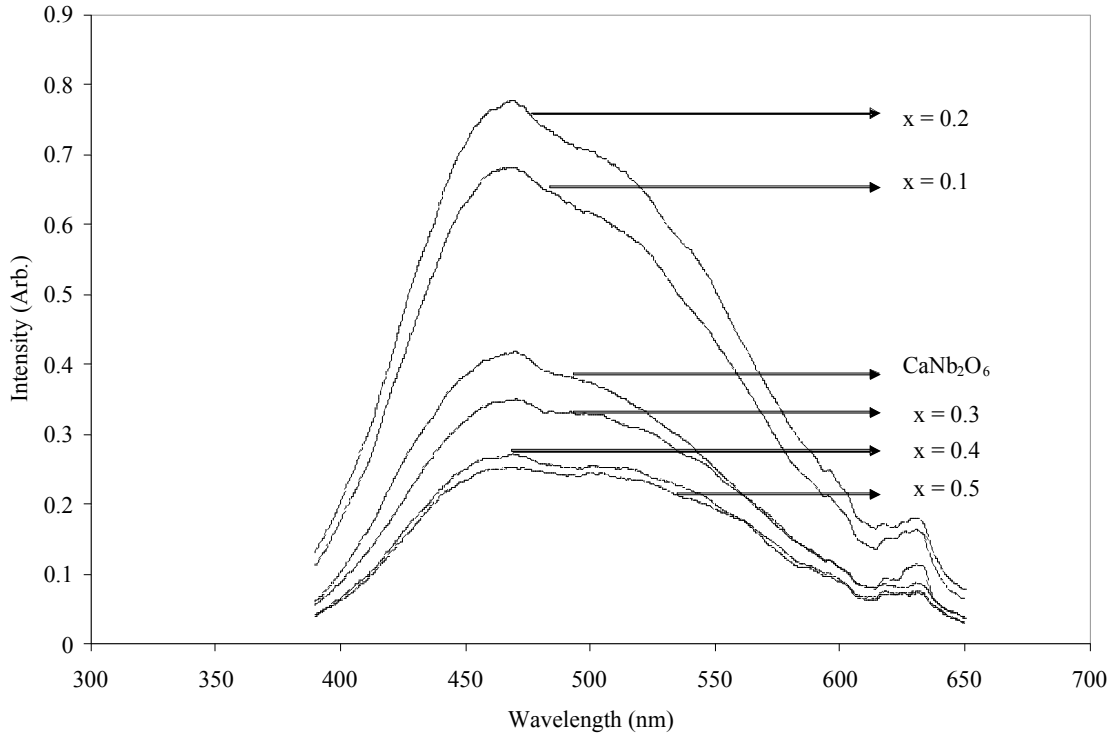

Figure 4.10. Photoluminescence spectra of $Ca_{1-x}Sr_xNb_2O_6$

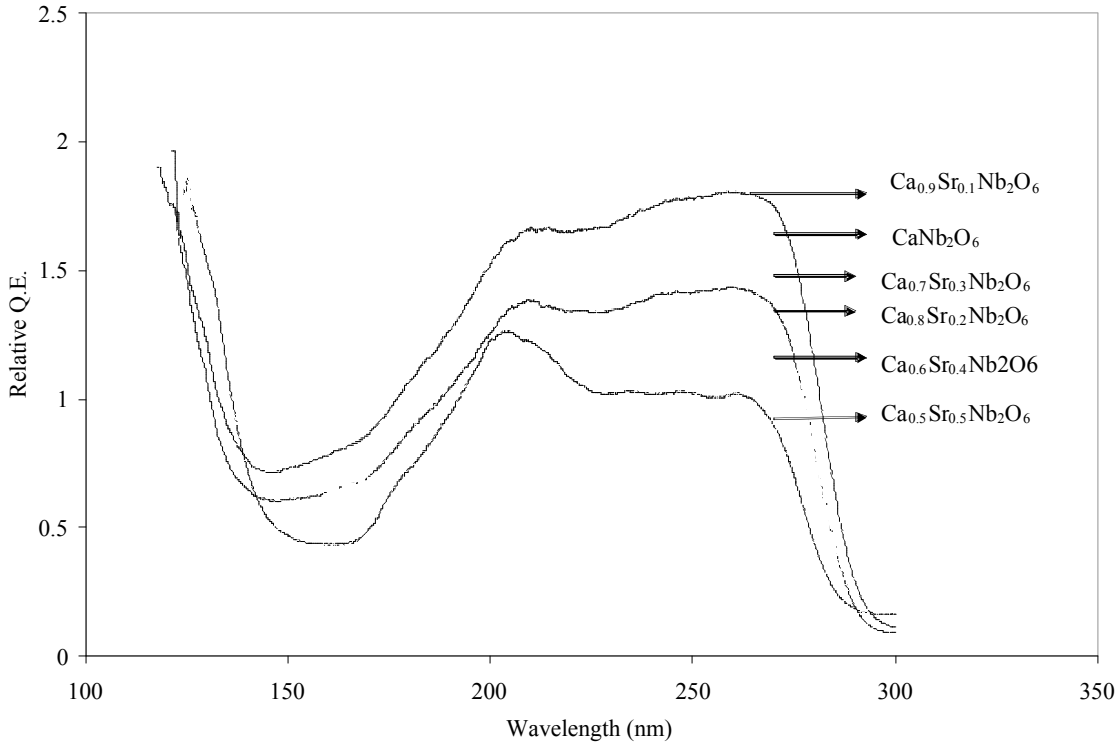

Figure 4.11. Photoluminescence excitation spectra of $Ca_{1-x}Sr_xNb_2O_6$

4.3.2. PL and PLE of $Ca_{1-x}Zn_xNb_2O_6$

The $Ca_{1-x}Zn_xNb_2O_6$ system has been investigated for x = 0 to x = 0.5. It is known that the Zn end member exhibits a blue luminescence under 254 nm that is very weak and is also included in the alloy system. The PL spectra for this system are shown in Figure 4.12. It was observed that the largest increase in intensity due to Zn substitution was for 10% Zn addition. This increase for x = 0.1 is by about 26% of the intrinsic emission (at 464.5 nm) as well as a peak shift to 475.5 nm. This is followed by the intrinsic $CaNb_2O_6$ emission at 464.5 nm and the x = 0.2 emission, which are approximately the same intensity, but where x = 0.2 shifts to 468.5 nm. A drastic decrease in intensity is observed between x = 0.2 and x = 0.3 and this could be explained by the XRD spectra in Figure 4.6. While the substitutions of x = 0.1 and x = 0.2 show spectra that are very similar to that of $CaNb_2O_6$, we observe a change in the pattern for x = 0.3 in which there is a large decrease in ratio of the primary $CaNb_2O_6$ peak with respect to the dominant $ZnNb_2O_6$ peak. Thus, the solid solution is continuous up to x = 0.2 after which there appears to be a precipitation of an intermediate phase that results in a reduction of the intensity. The emissions for samples with x = 0.3, x = 0.4 and x = 0.5 are nearly identical but show a very slight increase in the peak position to slightly higher wavelengths. The intrinsic $ZnNb_2O_6$ shows a primary broad band emission at 422.5 nm and a secondary broad band emission centered at 545 nm. However, as Zn is added, its secondary emission peak of 545 nm becomes progressively more dominant than that of the primary $CaNb_2O_6$ peak at 464.5 nm peak. Since the large increase in emission intensity for x = 0.1 could not have occurred as a result of any lattice expansion, we ascribe this increase to the Zn d electrons

which participate in the Nb^{5+} to O^{2-} charge transfer. Because $ZnNb_2O_6$ is only weakly luminescent and has two different emission peaks, we observe a decrease in emission intensity as we approach the Zn end member. Unfortunately, we also see a dominance in the 545 nm emission over the 464.5 nm peak for all Zn additions. Nevertheless, Zn substitution justifies the second approach outlined in the introduction, although the 545 nm emission would need to be somehow suppressed and the peak shifts should be to lower wavelengths.

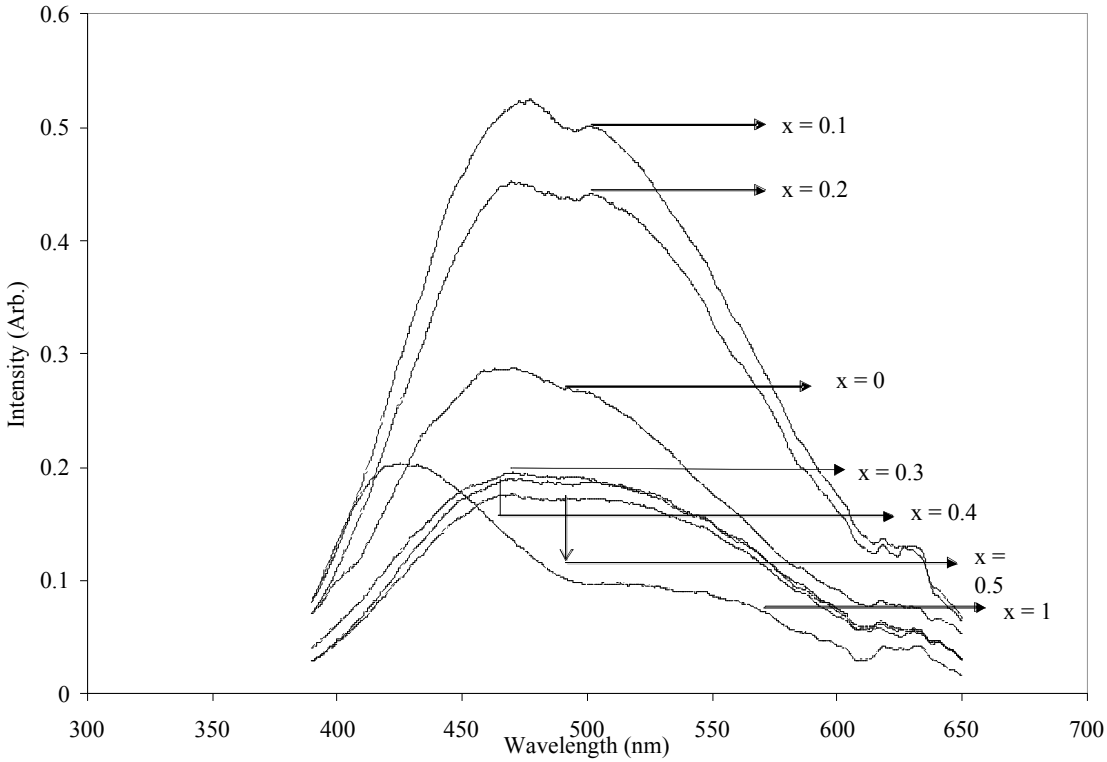

Figure 4.12. Photoluminescence spectra of $Ca_{1-x}Zn_xNb_2O_6$

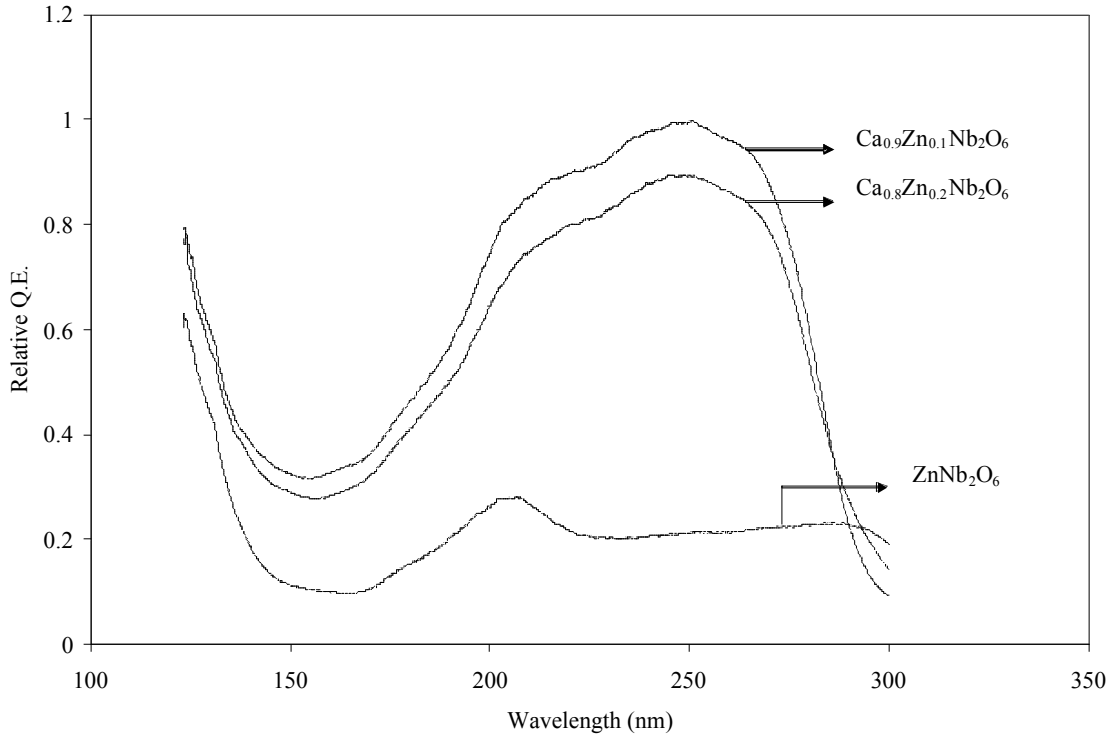

Figure 4.13. Photoluminescence Excitation spectra of $Ca_{1-x}Zn_xNb_2O_6$

4.3.3. PL and PLE of $CaNb_{2(1-x)}Ta_{2x}O_6$

The PL of the $CaNb_{2(1-x)}Ta_{2x}O_6$ system was investigated for Ta additions of x = 0, x = 0.1, x = 0.2, x = 0.3 and to x = 0.5. It can be observed from the PL spectra in Figure 4.14 and the PLE spectra in Figure 4.15 that the intrinsic luminescence of $CaNb_2O_6$ is reduced significantly by the addition of just 10 mol% of Ta (x = 0.1) and decreases systematically for x = 0.2 and x = 0.3, which are all continuous within the solid solution as proven by the XRD spectra in Figure 4.6. This quenching, which occurs by about 50% for x = 0.1, is unexpected as the addition of Ta was expected to affect the NbO_6^{2-} octahedron thereby increasing the emission intensity. It is unclear why the quenching occurs, although it has also been reported that substituting V (which is smaller

than Nb and belongs to the same group (VA) as Nb and Ta) into $CaNb_2O_6$ quenches the luminescence as well.[4] Thus, it appears that trying to control the luminescence by directly influencing the luminescent center adversely affects it. Thus, there is no reason to expect the Dubnium (Db), the last element in the group would have the effect of increasing the intensity. Furthermore, Db sources would be nearly impossible to obtain as it is a synthetic element that has never been isolated in observable quantities.[21]

The PLE of $CaNb_{2(1-x)}Ta_{2x}O_6$ for x = 0 and x = 0.1 is shown in Figure 4.15. The excitation spectra for these compositions both indicate excitation of the host lattice. However, the excitation maximum for x = 0.1 peaks at about 267 nm and decreases to lower wavelengths, while that of $CaNb_2O_6$ ranges approximately from about 207 nm to 267 nm. As in the PL spectra, the relative quantum efficiency of $CaNb_2O_6$ also decreases drastically for all the wavelengths of interest.

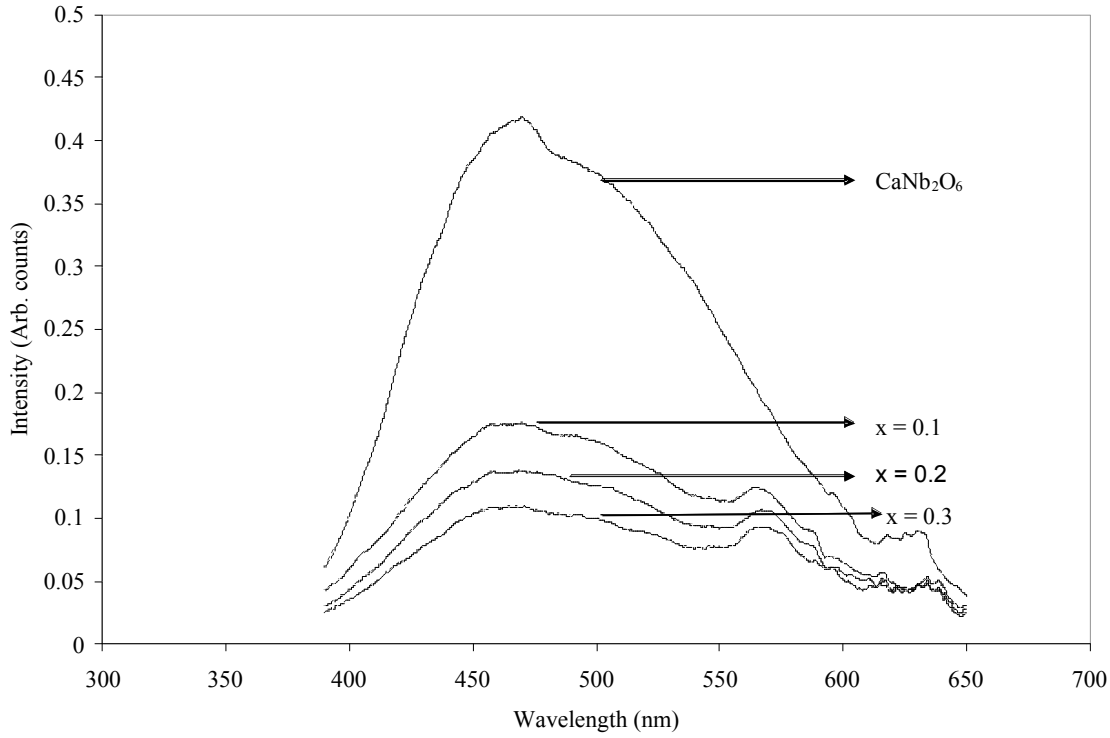

Figure 4.14. PL spectra of $CaNb_{2x}Ta_{2(1-x)}O_6$

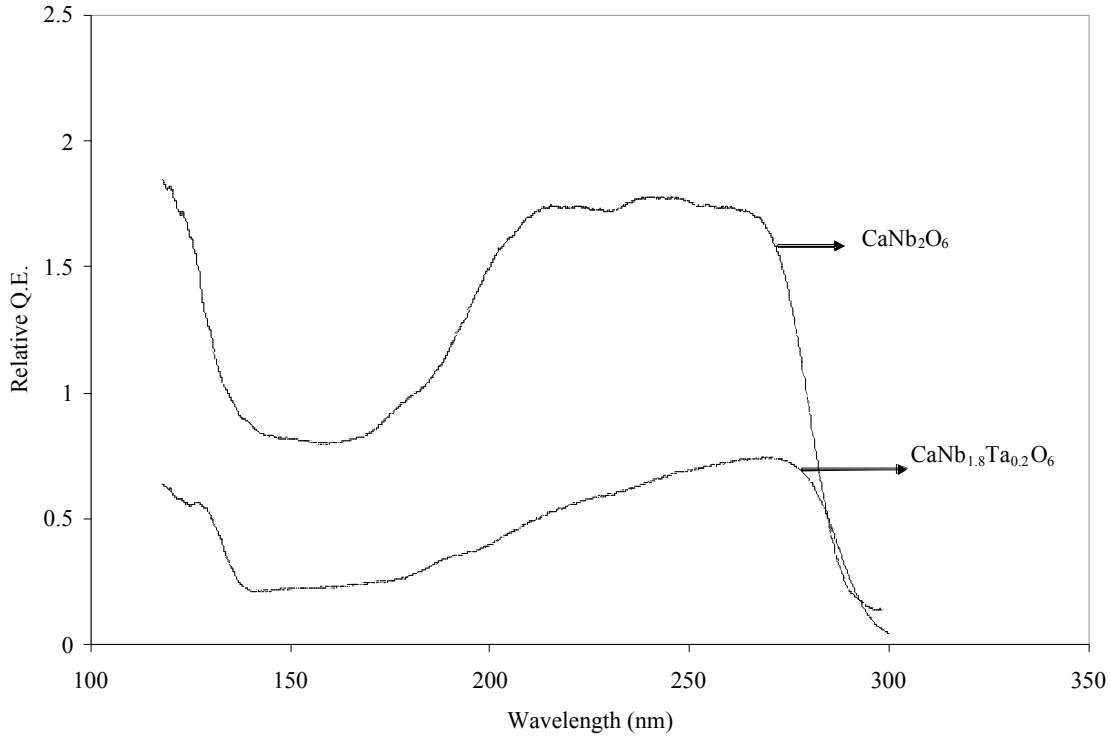

Figure 4.15. Photoluminescence excitation spectra of $CaNb_{2x}Ta_{2(1-x)}O_6$

4.3.4. PL and PLE of $Ca_{1-x}Ba_xNb_2O_6$

The effect of alloying Ba with $CaNb_2O_6$ is shown by the PL spectra of Figure 4.16. It is observed that for a 10 mol % addition of Ba, the PL intensity of $CaNb_2O_6$ is only increased by 3 %. As predicted, Ba^{2+}, being a larger ion than Ca^{2+}, causes the lattice to expand, thereby increasing the crystal field and the luminescence intensity. There is a large gap in intensity between x = 0.2 and x = 0.3 indicating a discontinuity in the solid solution or the precipitation of an additional phase, which is consistent with the XRD spectra in Figure 4.7. The reason why the lattice expansion due to x = 0.2 does not increase the PL intensity is that Ba^{2+} has a large ionic mismatch with Ca^{2+} which introduces stresses that compete with the crystal field, and can offset it if they are large enough. This effect is discussed more thoroughly in Chapter VI.

The PLE of the $Ca_{1-x}Ba_xNb_2O_6$ alloy for x = 0.1, x = 0.1 and x = 0.3 are shown in Figure 4.17. The discontinuity in the solid solution at x = 0.3 can be clearly observed for all the wavelengths investigated.

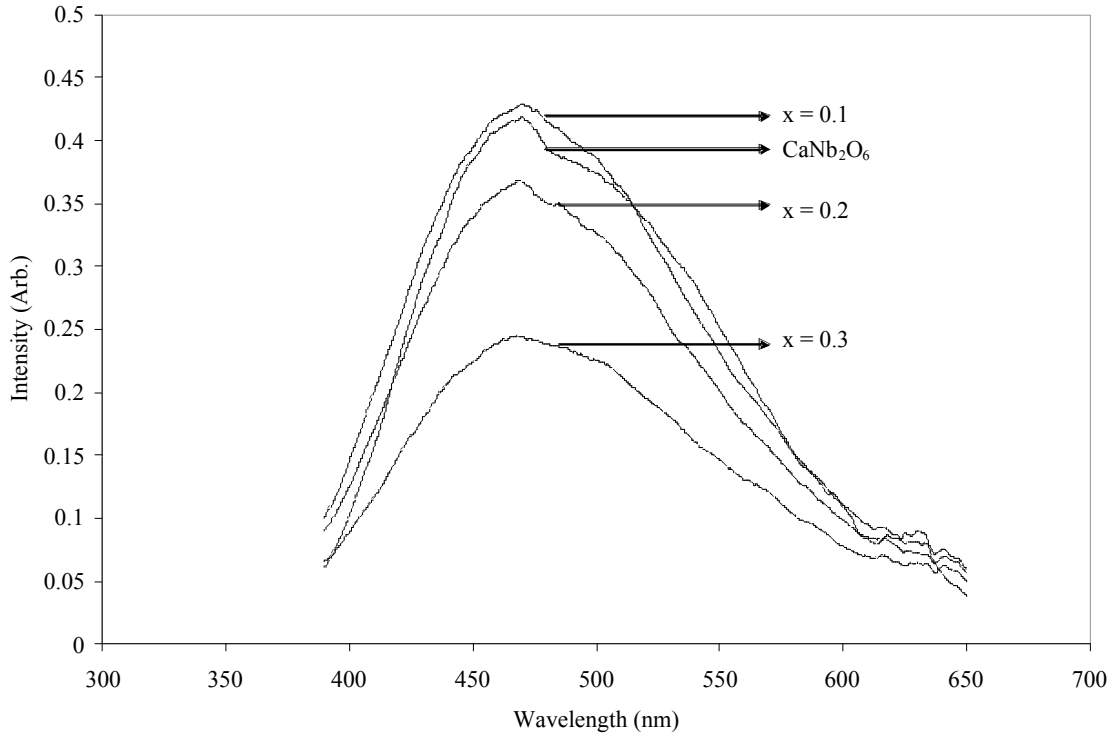

Figure 4.16. Photoluminescence spectra of $Ca_{1-x}Ba_xNb_2O_6$

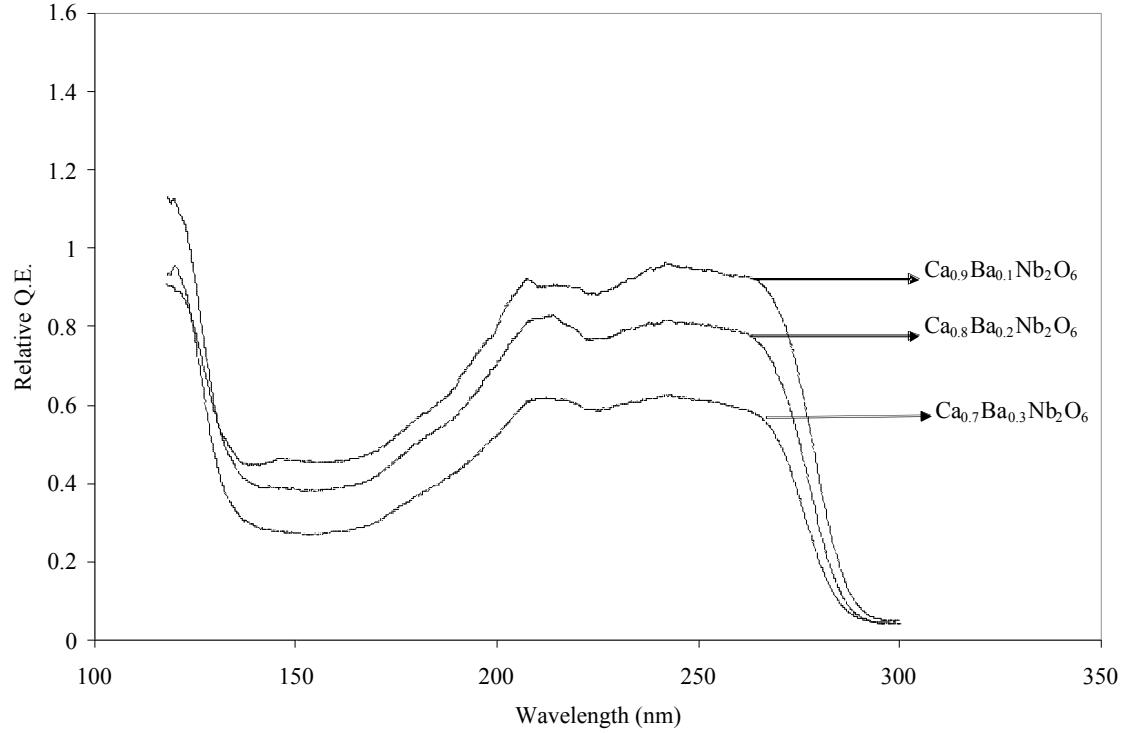

Figure 4.17. Photoluminescence excitation spectra of $Ca_{1-x}Ba_xNb_2O_6$

4.3.5. PL and PLE of $Ca_{1-x}Mg_xNb_2O_6$

Mg substitution into $Ca_{1-x}Mg_xNb_2O_6$ causes a contraction of the lattice, since Mg is a smaller atom than Ca. This contraction decreases the crystal field experienced by the $NbO6^{2-}$ octahedron, thereby reducing the luminescence intensity of $CaNb_2O_6$ as shown in the PL spectra of Figure 4.18. The substitution of x = 0.1 diminished the intrinsic intensity by about 13% and is further reduced for x = 0.2 and x = 0.3. We also observe peak shifts from 464.5 nm in $CaNb_2O_6$ to 468 nm for x = 0.1, 464 nm for x = 0.2 and finally to 466 nm for x = 0.3, showing no specific trend in the peak shifts with respect to Mg addition.

The PLE spectra shown in Figure 4.19 again show the host lattice excitation that is characteristic of the luminescent metaniobate compounds. For x = 0.1, we observe a conspicuous excitation maximum at 205 nm, while for x = 0.2 and x = 0.3, the excitation edge ranges from 200 nm to 260 nm.

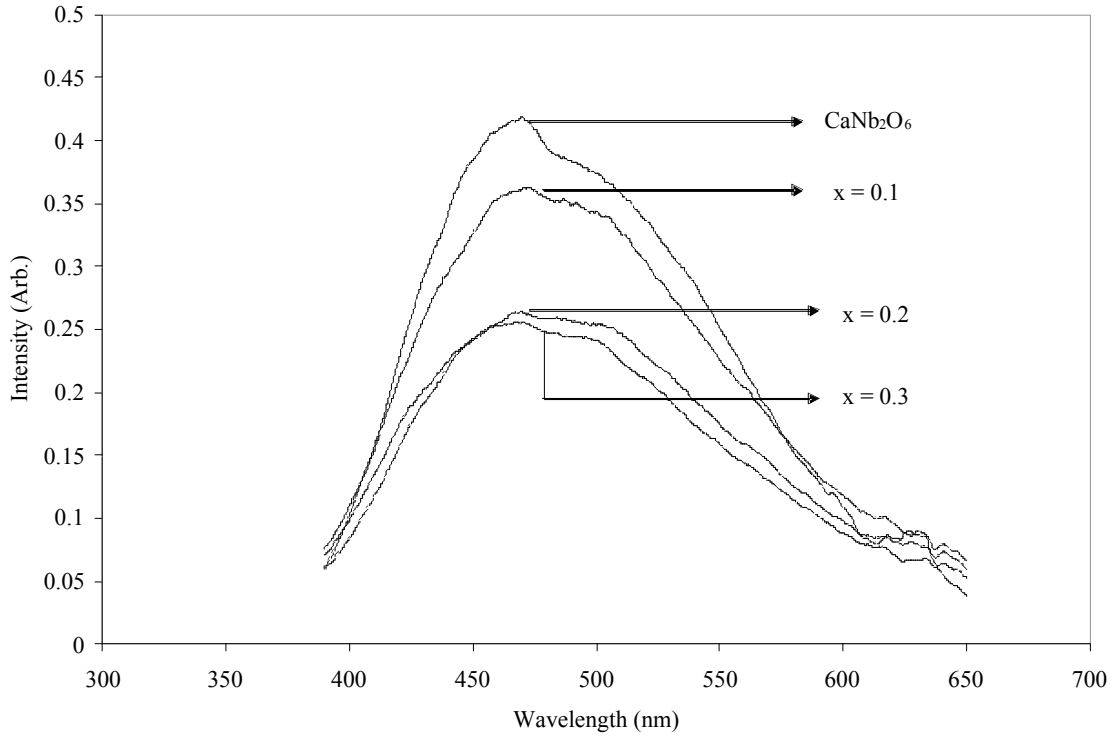

Figure 4.18. Photoluminescence spectra of $Ca_{1-x}Mg_xNb_2O_6$

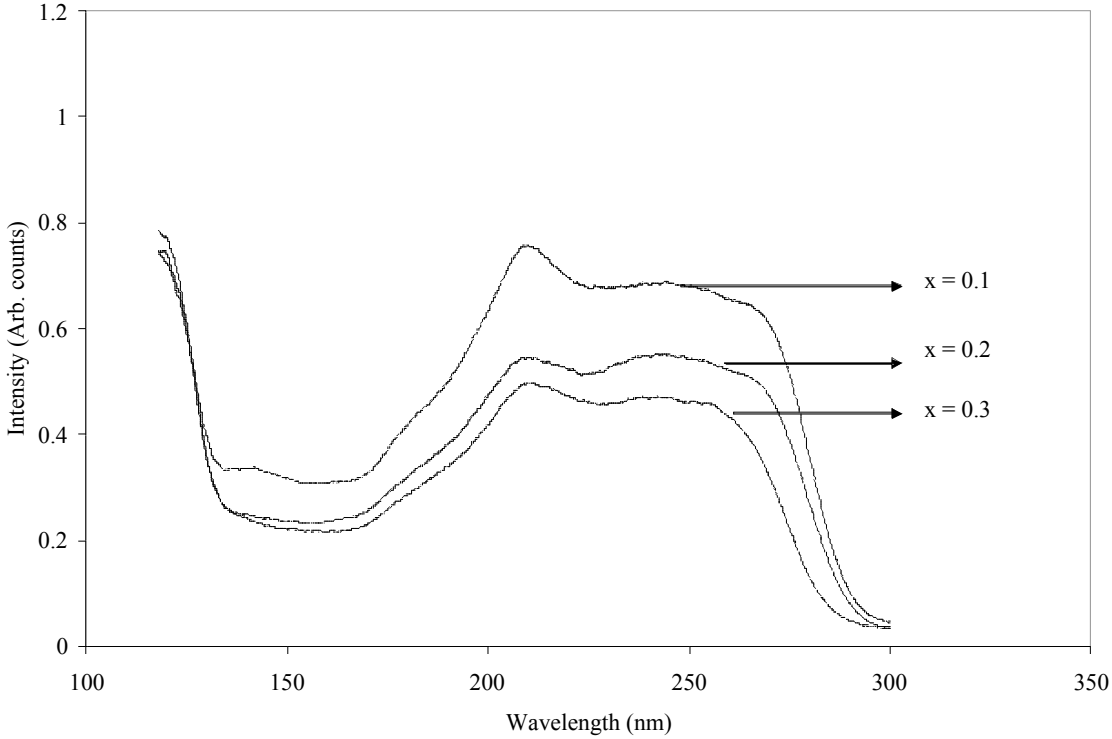

Figure 4.19. Photoluminescence excitation spectra of $Ca_{1-x}Mg_xNb_2O_6$

4.4. Morphology And Particle Size

The morphology of a phosphor powder sample has been studied under a LEO scanning electron microscope. SEM pictures of $Ca_{0.8}Sr_{0.2}Nb_2O_6$, the sample with the most intense PL and the best PLE are shown in Figure 3.1a and Figure 3.2b.

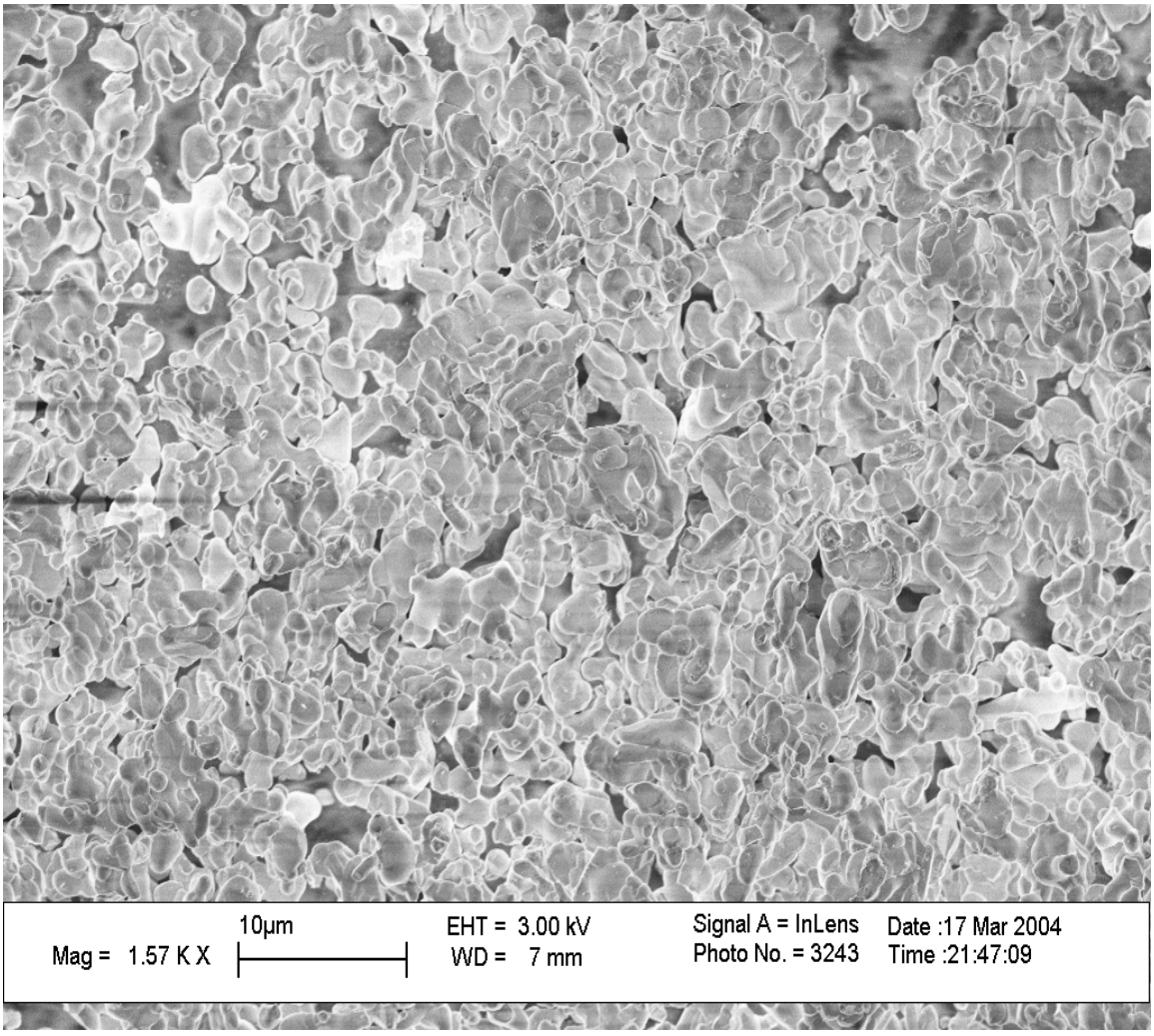

Figure 3.1a shows an SEM picture of $Ca_{0.8}Sr_{0.2}Nb_2O_6$ at 1570, X magnification showing loosely agglomerated particles.

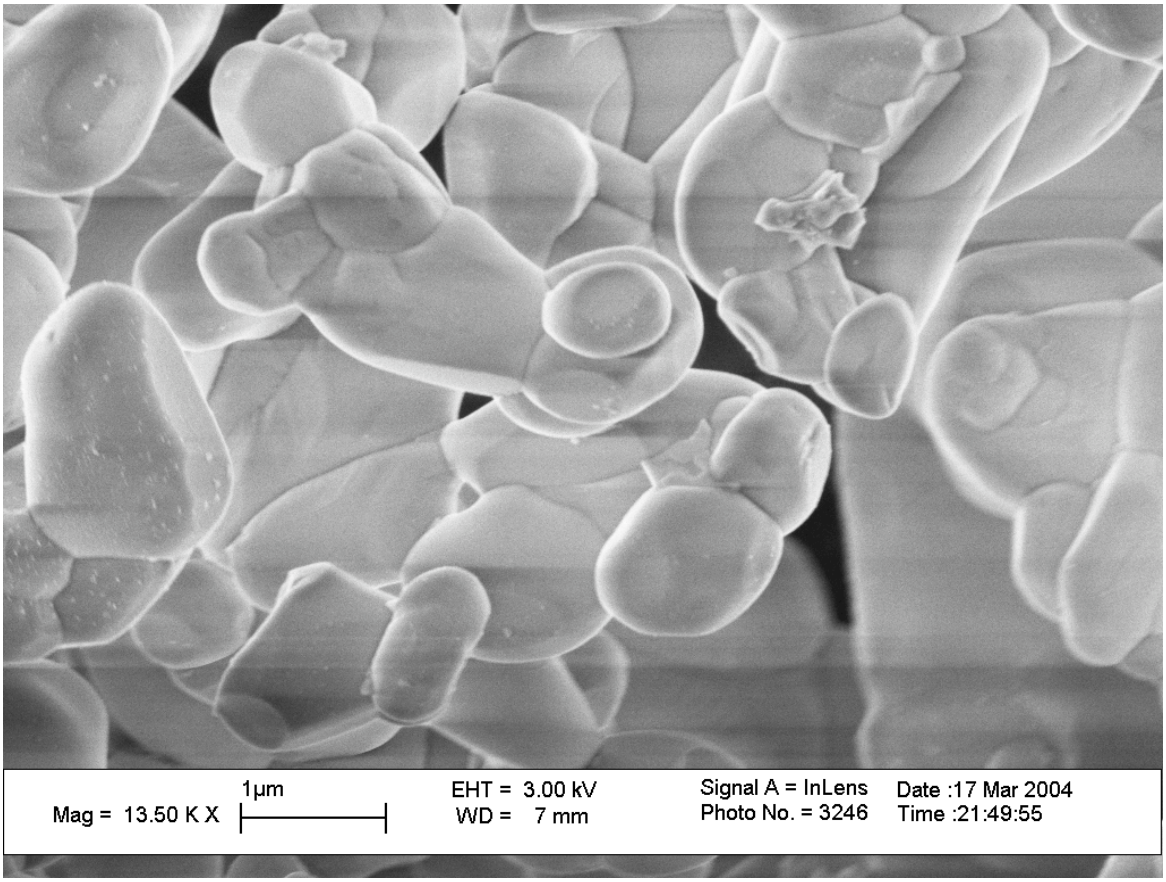

Figure 3.1b shows an SEM picture of $Ca_{0.8}Sr_{0.2}Nb_2O_6$ at 13,500 X magnification showing more distinct particles.

Figure 3.1a shows an image of powder particles that are loosely agglomerated, whereas Figure 3.1b shows more distinct particles that are reasonably well crystallized viewed at a closer range. However, while both figures show that the particles are irregular, with a slightly angular shape, it can be seen from Figure 3.1b that the surfaces are actually smooth. The average particle diameter is estimated to be between 0.5 _m and 3 _m. A more efficient size and shape, particularly for displays could likely be obtained by the use of a flux agent during the synthesis procedure. It has been reported that fluxes such as AlF_3 can be added to the starting mixture of phosphors before calcinations.[17]

CHAPTER V

CALCULATIONS

Section 5.1.

In general, the energy difference between the ground and excited energy levels at equilibrium, and a short time after excitation, is less than the energy difference at the instant of excitation, such that $E_e < E_a$. E_e, which represents the energy of the emitted photon is usually much less than E_a, which represents the energy of the absorbed photon and the statement that $h\_a \geq h\_e$ is known as Stokes' law.[16] The Stokes' shift is then calculated as the energy difference between the maximum of the lowest excitation band and the maximum of the emission band.

The $S < 5$, we are in the intermediate coupling scheme and for $S > 5$, we have the strong coupling scheme. S is proportional to $(\_R)^2$, where _R is the parabola offset, which determines the width of the optical spectra in a configurational coordinate diagram.[9] Thus, the larger the Stokes' shift, the broader the optical bands involved, and the higher the strength of the electron-lattice coupling, S.

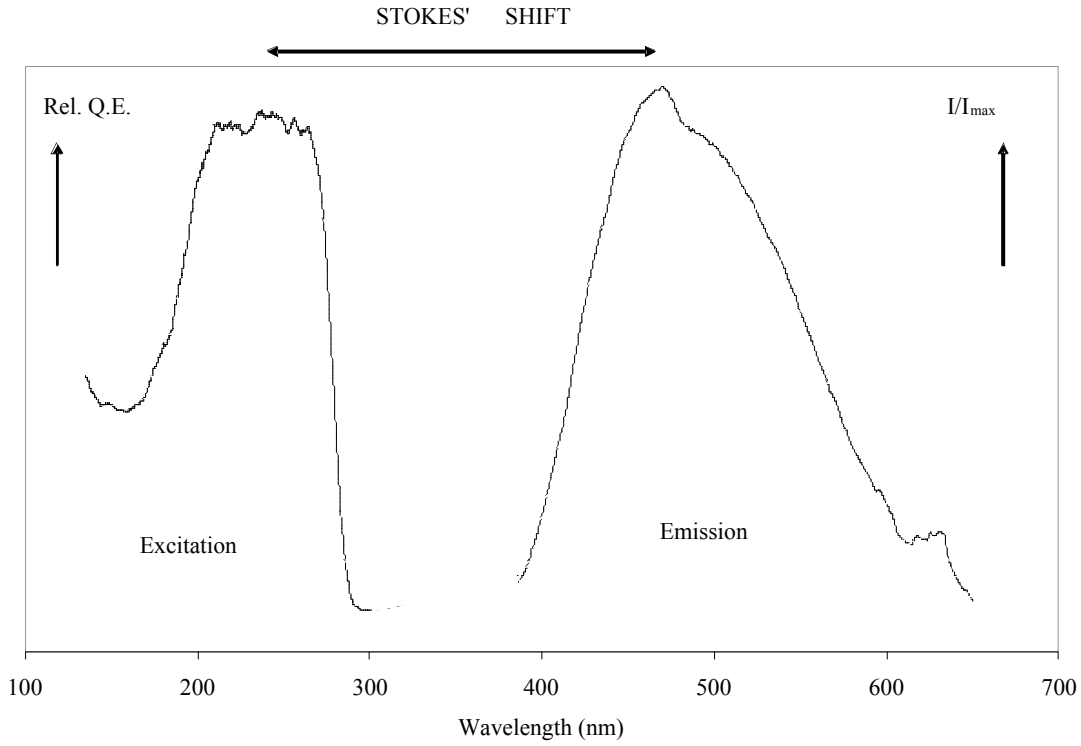

Figure 5.1 Excitation and emission spectra of the intrinsic luminescence of $CaNb_2O_6$ showing Stokes' shift.

Figure 5.1 above shows the normalized emission and excitation spectra of $CaNb_2O_6$, with an enormous Stokes' shift of about 39,100 cm^{-1}. This indicates a strong electron-lattice coupling, which is expected in self-activated phosphor whereby the absorption, energy transfer process and emission all occur within the same material. We calculate similarly large shifts for all the alloys of calcium metaniobate, which is expected as they are simply modifications of the crystal structure, as opposed to extrinsic activators. The strong electron-lattice coupling also shows that these phosphors would be more stable to harsh operational environment and the burn-in procedure used in the manufacture of plasma display panels. One reason is that $CaWO_4$, for example, which has a similarly large Stokes' shift is able to absorb X-rays and to convert the absorbed energy efficiently into a light and is a stable material used in x-ray screens.[25]

Section 5.2 CIE Chromaticity Coordinates

Standard functions for the three primary colors were determined in 1931 by the Commission Internationale de l'Eclairage (CIE), the International Commission on Illumination. Tristimulus functions were derived by determining the average response of the human eye. The spectral radiance associated with the three color functions were integrated in order to specify color. Thus,

$X = \int I(\lambda)x(\lambda)d\lambda$;

$Y = \int I(\lambda)y(\lambda)d\lambda$;

$Z = \int I(\lambda)z(\lambda)d\lambda$, where x($\lambda$), y($\lambda$), z($\lambda$) are tristimulus functions.

The chromaticity coordinates x, y, z, are then determined by normalizing each of the tristimulus functions such that

$$x = \frac{X}{X + Y + Z};$$

$$y = \frac{Y}{X + Y + Z};$$

$$z = \frac{Z}{X + Y + Z}, \text{ where } x + y + z = 1.$$

The chromaticity diagram shown in Figure 5.2 corresponds to wavelengths of spectrally pure colors and in bounded by the reduced x and y coordinates. The three primary colors red, blue and green, can be combined to produce the entire color gamut. For example, mixing red and blue gives purple, which is inside the boundary. White light has the coordinates x = 0.33, y = 0.33 and since the diagram does not represent intensity,

the absence of white is black and gray is all intensity scales in between, all being represented by the same point.

Table 5.1. The CIE coordinates of the spectrally pure colors, which are placed at the end points of the diagram

Color	X	y	Wavelength for line emission
Red	> 0.55	< 0.33	770 – 645 nm
Green	< 0.20	> 0.50	525 – 500 nm
Blue	< 0.15	< 0.15	480 – 465 nm
White	0.33	0.33	---

The CIE coordinates of our most intense sample, $Ca_{0.8}Sr_{0.2}Nb_2O_6$ were calculated using the Cie4 Fortran program. The coordinates were found to be x = 0.2295, y = 0.30467, z = 0.46582, which lies (as a small white square) on the edge of blue-green and leaning strongly to white, as compared to BAM, which is clearly in the blue region as shown in Figure 5.2.

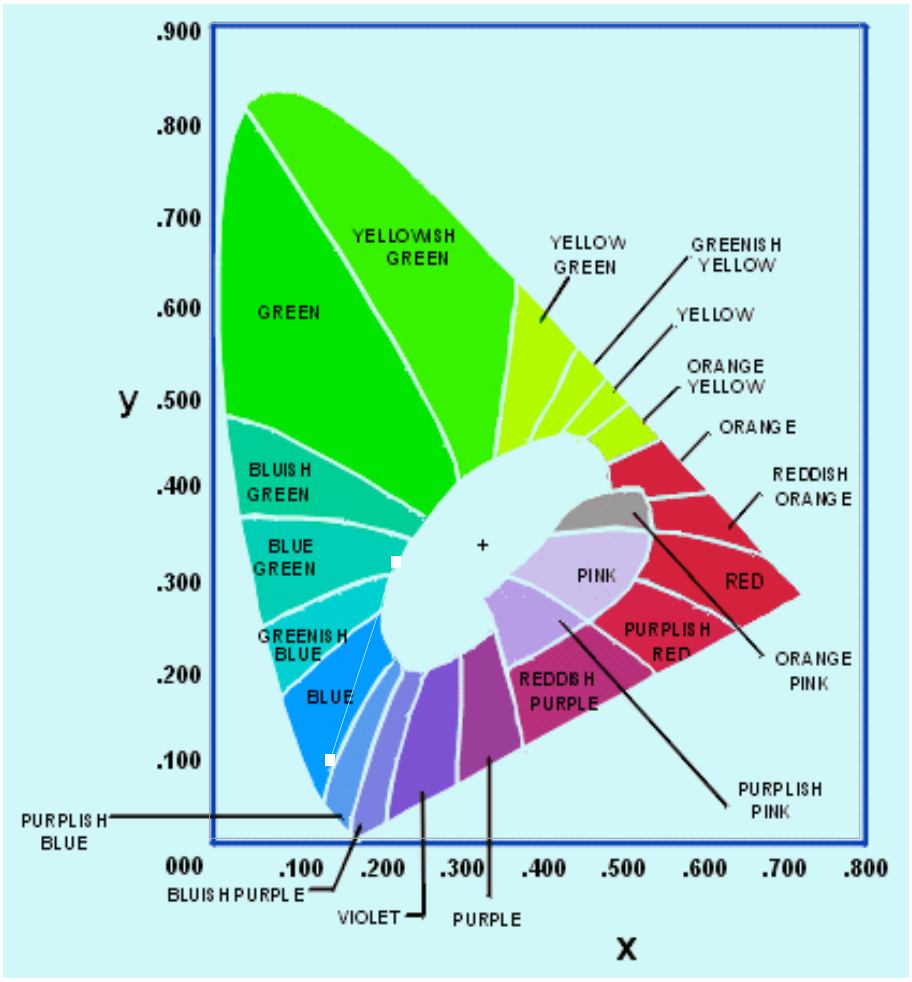

Figure 5.2 CIE chromaticity diagram showing coordinates of $Ca_{0.8}Sr_{0.2}Nb_2O_6$ (x = 0.2295, y = 0.30467) lying on the edge of blue-green and leaning strongly towards white, while BAM (x = 0.15, y = 0.086) strongly lies in the blue regime.

CHAPTER VI

DISCUSSION

6.1. Effect of Alloying on Structure

Alloying was performed on the self-activated $CaNb_2O_6$ to alter its structure and hence its luminescence. In the first approach, we alloyed $CaNb_2O_6$ with the alkali metals, Sr, Ba and Mg. As a consequence of the relative sizes of the atoms substituting for Ca^{2+} sites in the lattice, we were able to show that Sr and Ba substitution causes a lattice expansion that leads to an increase in the PL intensity, while Mg substitution causes a contraction of the lattice, which leads to a decrease in the PL intensity. Furthermore, due to the greater ionic mismatch between Ca^{2+} and Ba^{2+} (26.7%) as compared to the mismatch with Sr^{2+} (14%), it is clear that Sr substitutes optimally into the Ca^{2+} sites as required by the Hume-Rothery rules for the formation of substitutional solid solutions. These rules require no more than a 15% size difference between the solute and the solvent, as well as similar valences, crystal structures, and comparable electronegativites.[13] Thus, the ionic mismatch with Ba^{2+} (26.7%) generates a stress which can be defined as a Type II stress, according to Kasano et al. because it results from the ionic mismatch between the host cations.[14] On the other hand, a Type I stress results from a mismatch between the host cations and substituting activator cations, and refers to the expansion or contraction of the parabola offset, _Q of a configurational coordinate diagram (not specifically discussed in this thesis). [15] However, as the host lattice both absorbs and emits the radiation in the $CaNb_2O_6$ phosphor we deduce that the Type II stress causes an expansion or contraction of the lattice around the luminescent

octahedron, NbO_6^{2-}. Substitution of smaller Mg^{2+} cations into the larger Ca^{2+} sites results in an ionic mismatch of 34 % that leads to a decrease in solubility in the alloy. This also causes a contraction of the lattice surrounding the luminescent ion, thus reducing the crystal field it experiences.

In the $Ca_{1-x}Zn_xNb_2O_6$ system, Zn^{2+} (0.74 A°) substitution into Ca^{2+} (0.99 A°) causes an ionic mismatch of 25% leads to a reduction of its solubility within the alloy, as well as a contraction of the lattice and a reduction of the crystal field experienced by the luminescent ion. Nevertheless, Zn was used because it has d electrons that can participate in the charge transfer process thereby offsetting the crystal field effect. Furthermore, substituting with Cd^{2+} (0.97 A°) would virtually eliminate these stresses so that the luminescence in primarily due to the Cd d electrons participating in the charge transfer. Alloying with Hg^{2+} (1.10 A°) would cause a lattice expansion similar to Sr, not only resulting in an increased crystal field but also in an increased participation in the charge transfer process due to the Hg d electrons.

The effect of Ta addition in the $CaNb_{2-x}Ta_xO_6$ does not seem to have a significant effect on the crystal structure, since both end members of the solid solution are columbite, and the intermediate compositions result in rynersonite, a close structural relative of columbite. There is no ionic mismatch, since the sizes of Ta^{5+} and Nb^{5+} in the 6-coordinate, octahedral configuration of the luminescent centers NbO_6^{2-}, and TaO_6^{2-} are both 0.78 A°. Thus, Ta substitution seems to have very little effect on the crystal structure but has a detrimental effect to the luminescence as will be discussed in the next section.

6.2. Effect of Alloying on Luminescence

The effect of alloying on the luminescence of metaniobate compounds has been shown to be very sensitive to the structural changes associated with it, which were discussed in the previous section. Sr substitution in the $Ca_{1-x}Sr_xNb_2O_6$ shows PL spectra in Figure 4.6 that are exactly analogous to the XRD spectra in Figure 4.4. The solid solution is continuous up to x = 0.2 which causes a lattice expansion and an increase in the crystal field that is clearly observable as an increase in the PL intensity of $CaNb_2O_6$. This intensity is increased by about 95% for x = 0.1, and by about 65% for x = 0.2. We then observe a steady decrease in the intrinsic intensity by 15% for x = 0.3 and decreasing further for x = 0.4 and x= 0.5.

The $Ca_{1-x}Ba_xNb_2O_6$ solution appears to be continuous up to x = 0.2 from the XRD spectra in Figure 4.7. However, a Type II stress occurs due to the ionic mismatch of Ba and Ca, which then competes with the increased crystal field that had resulted from the lattice expansion. Thus, from the PL spectra in Figure 4.11, we observe that the increased intensity due to the crystal field for x = 0.1 was sufficient to offset the effect of the Type II stress but the net increase was only about 3%. On the other hand, while the x = 0.2 substitution is still continuous in the solid solution, the Type II stresses have been increased and are able to offset the effect of the crystal field so that we observe a reduction in the intrinsic PL intensity of $CaNb_2O_6$. We then observe a large decrease in the PL intensity at x = 0.3 with respect to x = 0.1 and x = 0.2, as well as the

corresponding differences in relative quantum efficiencies from the PLE, thereby indicating a discontinuity in the solid solution. Thus, while the stresses that occur in this system compete adversely against the PL intensity of this system, we are still able to obtain useful information on the structural changes from the PL and PLE spectra.

Addition of Mg into the $Ca_{1-x}Mg_xNb_2O_6$ system causes a contraction of the lattice and a decrease in the crystal field experienced by the luminescent ion as stated in section 6.1. The ionic mismatch between Mg and Ca also causes a reduced solubility which combines with the diminished crystal field to significantly reduce PL intensity of the intrinsic emission.

Zn substitution into the $Ca_{1-x}Zn_xNb_2O_6$ system also causes a contraction of the lattice and a reduction of the crystal field as stated previously. However, its d electrons enhance the luminescence intensity by participating in the charge transfer within the NbO_6^{2-} octahedron, a process which allows it to overcome both the reduction of the crystal field and a drastic reduction in solubility after x = 0.2 that results from the ionic mismatch. Thus for x = 0.1 and x = 0.2, we observe and increase in the intrinsic metaniobate intensity, followed by a large decrease from x = 0.3 which is associated with a discontinuity in the solid solution as confirmed by the XRD spectra. Also, as mention in Section 6.1, Cd addition would have virtually no effect of Type II stresses, while Hg would cause a lattice expansion that would offset a small effect of the stresses, which when combined with their d electrons should increase the photoluminescence intensity more dramatically than the Zn alloys. Unfortunately, those studies have not yet been pursued due to time restrictions.

It is difficult to explain why Ta addition reduces the intrinsic luminescence of $CaNb_2O_6$ although this is a different situation which does not alter the cuboid of Ca atoms surrounding the NbO_6^{2-} octahedra, but tries to affect the luminescent center itself. It is known from the ionic radii and electronic structure, that the sizes of Nb and Ta are very similar and that Nb contributes more d electrons than Ta that could participate in the charge transfer. Thus, since $CaTa_2O_6$ is only weakly luminescent and Ta itself does not positively influence Nb, this is a possible explanation why the PL intensity and efficiency is reduced. Another possibility is that since the luminescence occurs as a direct result of the transitions between O^{2-} ions from the valence band and Nb^{5+} ions in the conduction band of the luminescent center, an addition of Ta^{5+} ions into the conduction band would compete against the transitions with Nb^{5+} ions, thus quenching the luminescence.

CHAPTER VI

CONCLUSIONS

The goal of the research presented in this thesis was to investigate the photoluminescence properties of $CaNb_2O_6$ when irradiated with high energy, 147 nm excitation for possible use as a blue component plasma display phosphor. The calcium metaniobate was found to be exhibit a blue self-activated luminescence and so it was necessary to find ways to increase its photoluminescence intensity. Eu^{3+}, which produces a red emission was incorporated into the host structure but unfortunately, all attempts to reduce it to the blue Eu^{2+} were unsuccessful. Thus, the only method of improving its intrinsic luminescence was to modify the crystal structure of the host lattice, as both absorption and emission processes occur within the same structure in self-activated phosphors. The structure was then modified and the dependence of the luminescence on structure was investigated in a comprehensive manner.

It is well known that while the components of a continuous solid solution have the same crystal structure, the compositional changes cause a change in the lattice parameter, which leads to an expansion or a contraction of the lattice. However, it has also been shown in this study, that the self-activated luminescence of calcium metaniobate can be drastically increased by alloying it with other elements. It was found that alloying with the alkali earth metals causes changes in the structure associated with the substituting element that leads to increases or decreases in the photoluminescence intensity and relative quantum efficiency. Sr and Ba, which are larger atoms than Ca, cause an expansion in the lattice leading to in increase in the crystal field experienced by the

luminescent center, the NbO_6^{2-} octahedron. Thus, for small additions that were continuous within the solid solution, we observed large gains in the photoluminescence intensity. The addition of 20 mol % Sr, for example approximately doubled the intensity of $CaNb_2O_6$, while a 10 mol % addition Sr increased it by about 65%. A 10 mol % addition of Ba also increased the intrinsic luminescence, but only by about 3 %. This was due to Type II stresses which were generated as a result of the ionic mismatch between Ba^{2+} and Ca^{2+} ions, that negated the increase cause by the lattice expansion. Mg on the other hand is smaller than Ca, which led to a contraction of the lattice, thus a decrease in the crystal field experienced by the luminescent center. This caused a reduction in intensity for all the substitutions that were continuous within the solution range, and precipitation of non-luminscent or weakly luminescent intermediate phases outside of it.

Secondly, it was shown that elements that have complete electron shells with large amounts of d electrons, such as Zn and Cd can contribute significantly to the luminescence, irrespective of their closeness in size to Ca. Such atoms allow their d electrons to participate in the charge transfer process between the O^{2-} orbitals in the valence band and the Nb^{5+} orbitals of the conduction band within the luminescent octahedron. The difference in size between Zn and Ca reduces the contribution of the d electrons, but atoms such as Cd and Hg that match better should show more dramatic gains in intensity.

Lastly, it was found that trying to directly affect the luminescence of $CaNb_2O_6$ by alloying with Ta exhibited led to concentration quenching of the luminescence. The same effect has been reported in the literature due to the incorporation V in Ta sites. One reason this occurs is that since the Ta^{5+} orbitals directly participate in the transitions with

the O^{2-} orbitals as well, this introduces a competitive effect with the Nb^{5+} orbitals, which causes the concentration quenching especially since the $CaTa_2O_6$ end member exhibits a much weaker luminescence than $CaNb_2O_6$.

Morphology and particle size analysis were also done by SEM. It was observed that while the particles are smooth and reasonably well crystallized, the particle sizes are not uniform and the shapes are uneven. Therefore, an improved synthesis procedure could help to make the particles more even or spherical and make the sizes more uniform within the powder, which would lead to additional gains in the photoluminescence efficiency and intensity. This can be done by adding a flux agent to the reactants before calcinations. The CIE coordinates of the best sample investigated, $Ca_{0.8}Sr_{0.2}Nb_2O_6$ was found to be x = 0.2295, y = 0.30467 which lies on the border between blue-green and white. The PL intensity was found to be 28% of that of BAM and the relative luminosity or photoptic vision was calculated to be 265.4128.

Finally, while the photoluminescence characteristics of the calcium metaniobate system still does not allow it the replace the commercial BAM used as the blue component plasma displays, it is more efficient at some wavelengths other than 147 nm. Its CIE coordinates are closer to white and it is more stable to the burn-in procedure used in panel manufacture than BAM due to its strong electron-lattice coupling as indicated by its enormous Stokes' shift. Thus, it has the possibility of being used in other applications such as in high energy lamps for lighting.

REFERENCES

1. Blasse, G. and Brixner, L.H., "Luminescence of Perovskite-like niobates and tantalates". Mat. Res. Bull. 1989: Vol. 24, pp. 363-366
2. A.M. Srivastava , J.F. Ackerman and W.W Beers, "On the Luminescence of $Ba_5M_4O_{15}(M=Ta^{5+},Nb^{5+})$".

   Journal of Solid State Chemistry. 1997: Vol. 134, 187-191. Article SC977574
3. Cummings, J.P. and Simonsen, S. H. "The crystal structure of calcium niobate ($CaNb_2O_6$). The American Mineralogist. 1970: Vol. 55, pp.90-97
4. Wachtel, A. "Self-Activated Luminescence of M^{2+} Niobates and Tantalates". Journal of the Electrochemical Society. 1964: Vol. 111, pp.534-538
5. Van Der Voort, D., de Rijk, J.M.E., Blasse, G. "Possibilities to Design a Cheap Red Lamp Phosphor. A study of $CaNb_2O_6:Eu^{3+}$". Physica Status Solidi 1993: Vol 135, pp.621-626
6. Blasse, G. and van Leur, M.G.J. "Luminescence and Energy Transfer in the Columbite Structure". Materials Research Bulletin. 1985: Vol 20, pp. 1037-1045.
7. McAllister, W.A. "Rare Earth-Activated Niobates". Journal of the Electrochemical Society.1984: Vol 131, pp.1207-1211.
8. Brixner, L.H., "On the Structural and Luminescent Properties of the $ScTa_{1-x}Nb_xO_4$ System".

   Journal of Chemical Education. 1980: Vol 57, pp. 588-590.

9. Blasse, G. and Grabmaier, B.C., "Luminescent Materials". Springer. Verlag Berlin Heidelberg. 1994.
10. Barendswaard W., Van der Waals, J.H. Molecular Physics. 1989: Vol 67, pp. 651
11. Vij D.R., Shionoya S., "Luminescence of Solids" Plenum Press, 1998.
12. Ropp R.C., "Studies in Inorganic Chemistry: 12, Luminescence and the Solid State". Elsevier Science Publishers B.V., 1991.
13. Schaffer J.P., Saxena A., Antolovich S.D., Sanders T.H., Warner S.B., "The Science and Design of Engineering Materials, Second Edition" WCB/McGraw-Hill, 1999.
14. Kasano H., Megumi K. and Yamamato J., "Japanese Journal of the Electrochemical Society. 1980: Vol 131, p. 1955
15. Edris Mohammed, Ph.D. Thesis, Georgia Institute of Technology. October 2000.
16. Leverenz, H.W., "An Introduction to Luminescence of Solids" John Wiley & Sons / Chapman & Hall, 1950.
17. Kubota S. and Shimada M., "$Sr_3Al_{10}SiO_{20}:Eu^{2+}$ as a Blue Luminescent Material for Plasma Displays". "Applied Physics Letters. Vol. 81, No. 15, pp. 2749-2751".
18. Cullity, B.D., "Elements of X-ray Diffraction" Addison-Wesley Publishing Company Inc., Philipinnes Copyright, (1978).
19. Richard Gilstrap, M.S. Thesis, Georgia Institute of Technology. July 2003.

20. Zeinally A.Kh., Lebedeva N.N., Mordukhayev A.R., and Mohamed A. Osman. "Photoluminescence of Barium Strontium Niobates and Strontium Pyroniobate". Ferroelectrics. 1982. Vol. 45, pp. 83 – 88.
21. URL: http://www.webelements.com/
The University of Sheffield and WebElements Ltd., UK. Copyright 2003.
22. Ishizawa N. and Marumo F., "The Crystal Structure of Sr2Nb2O7, ac Compound with Perovskite-Type Slabs". Acta Crystallographica. 1975. Vol. B31, pp. 1912.
23. Krupa J.C. and Queffelec M., "UV and VUV optical excitations in wide band gap materials doped with rare earth ions: 4f-5d transitions". Journal of Alloys and Compounds. 1997. Vol. 250, pp. 287 – 292.
24. Jüstel T., Krupa J.C., Wiechert D.U, "VUV spectroscopy of luminescent materials for plasma display panels and Xe discharge lamps". Journal of Luminescence. 2001. Vol. 93, pp. 179 – 189.
25. Kitai A.H., "Solid State Luminescence: Theory, Materials and Devices" Chapman and Hall, U.K. 1993.
26. Goldberg J. and Newbury D., "Scanning Electron Microscopy and X-ray Microanalysis". Plenum Press, NY. 1992.